QUANTIFYING THE INTRACELLULAR METABOLIC NETWORK THAT ESTABLISHES THE SIMULTANEOUS UTILIZATION OF SUGARS AND AROMATIC SUBSTRATES IN PSEUDOMONAS PUTIDA KT2440

A Thesis
Presented to the Faculty of the Graduate School
of Cornell University
In Partial Fulfillment of the Requirements for the Degree of
Master of Science

by
Matthew Alexander Kukurugya
January 2017

Abstract

The ability of *Pseudomonas* to use both aromatic compounds and sugars is being explored and exploited for emerging biotechnological applications, such as bioremediation as well as biofuel and chemical synthesis. The present study investigates the intracellular metabolism in the biotechnologically-important soil bacterium *Pseudomonas putida* KT2440 during feeding on a mixture containing the cellulosic hexose sugar (glucose) and an aromatic carboxylic acid (benzoate). Through a combination of ^{13}C tracer experiments with metabolic flux analysis (MFA), I elucidated and quantified the discriminate metabolic routing of each substrate throughout central carbon metabolism. The results determined that glucose-derived carbon was primarily routed to the Entner-Doudoroff (ED) pathway, reverse Embden–Meyerhof–Parnas (EMP) pathway, and Pentose Phosphate (PP) pathway, while benzoate-derived carbon was routed almost exclusively to the tricarboxylic acid (TCA) cycle. I found that benzoate catabolism influenced the routing of glucose in the ED pathway, reverse EMP pathway, and PP pathway, despite the absence of benzoate-derived carbon in these pathways. In the TCA cycle, the simultaneous catabolism of benzoate and glucose led to the activation of the glyoxylate shunt. Accordingly, kinetic isotopic flux revealed a decreased flux through isocitrate dehydrogenase and α-ketoglutarate dehydrogenase. In addition, feeding on the substrate mixture induced carbon overflow from the TCA cycle primarily through a significant involvement of malate dehydrogenase activity over the ED pathway in the biosynthesis of pyruvate. In sum, the data revealed that a preferential flux of substrate-derived carbons through different metabolic pathways was necessary to optimize biomass growth. These findings will contribute to an emerging framework for understanding soil carbon metabolism and advancing novel biotechnological applications in soil bacteria.

BIOGRAPHICAL SKETCH

Matthew A. Kukurugya earned his Bachelor of Arts degrees in Biochemistry and Political Science from DePauw University in 2013. From 2013 – 2014, he traveled to Latin America to conduct research in the Costa Rican rainforest and volunteer on a Peruvian organic farm. In 2014, he joined the Biological and Environmental Engineering graduate program at Cornell University under the supervision of Dr. Ludmilla Aristilde. He was also mentored by Dr. Janice Thies and Dr. Anthony Hay, who served as minor committee members for his MS thesis.

ACKNOWLEDGEMENTS

I sincerely and deeply thank Dr. Ludmilla Aristilde for her guidance throughout my MS. I also acknowledge the mentorship of both Dr. Janice Theis and Dr. Anthony Hay. In addition, I thank all of the current and past members of the Aristilde lab for their friendship and support. I especially thank Samantha Sasnow. Without all of her previous work, this research would not be possible. I also thank Dr. Ivan Keresztes and Anthony Condo of Cornell NMR Facility for their irreplaceable wisdom and help. I thank my family and friends for their constant encouragement, especially my incredible housemates over the past two years. Finally, I acknowledge the music of Stephen Malkmus and The Jicks, Manu Chao, The Red Hot Chili Peppers, Toots and The Maytals, Rage Against the Machine, Donavon Frankenreiter, Wilco, Sonny Rollins, Grant Green, Frederic Chopin, Phillip Glass, and Moby for providing inspiration during my writing and data analysis.

TABLE OF CONTENTS

LIST OF FIGURES

LIST OF TABLES

LIST OF ABBREVIATIONS

G6P	Glucose-6-phosphate
F6P	Fructose-6-phosphate
FBP	Fructose-1,6-bisphosphate
DHAP	Dihydroxyacetone phosphate
GAP	Glyceraldehyde-3-phosphate
3-PG	3-phosphoglycerate
PEP	Phosphoenolpyruvate
Pyr	Pyruvate
AcCoA, acetyl-CoA	Acetyl coenzyme A
S7P	Sedoheptulose-7-phosphate
R5P	Ribose-5-phosphate
E4P	Erythrose-4-phosphate
OAA	Oxaloacetate
α-KG	α-ketoglutarate
Gln	Glutamine
Glucn	Gluconate
α-KGDH	α-ketoglutarate dehydrogenase
ICDH	Isocitrate dehydrogenase
SDH	Succinate dehydrogenase
PEP carboxykinase	Phosphoenolpyruvate carboxykinase
MALDH	Malate dehydrogenase

CHAPTER 1: INTRODUCTION

Pseudomonas putida is a gram-negative bacterium that can thrive in diverse nutritional environments, including soil and aquatic matrices, due to its diverse metabolic capabilities (Palleroni et al.,1984; Basu et al. 2006; del Castillo et al., 2007; Sudarsan et al., 2014). In the rhizosphere, *P. putida* is considered a beneficial bacterium that produces plant growth-promoting hormones, such as indole-3-acetic acid (Glick et al.,1996). Several strains of *P. putida* have been investigated within the context of bioremediation of benzene contaminants (e.g., xylene, styrene, chlorinated and methylated benzene) (Rojo et al.,1987; Schmidt et al., 2001; George and Hay, 2012; Poblete-Castro et al., 2012) and the production of valuable chemicals including pharmaceuticals (Poblete-Castro et al., 2012; Vardon et al., 2015). Strains of *P. putida* have also been highlighted for their abilities to break down lignocellulose, a potential biofuel feedstock (Bugg et al., 2011; Fang et al., 2012; Palazzolo and Kurina-Sanz, 2016). Therefore, the cellular physiology of *P. putida* as a model bacterium is of considerable interest with respect to biotechnological applications (Bugg et al., 2011; Poblete-Castro et al., 2012; Vardon et al., 2015; Nikel et al., 2016; Johnson et al., 2016; Palazzolo and Kurina-Sanz, 2016).

Here is a detailed investigation of the metabolic network structure in *P. putida* KT2440 that underpins the co-metabolism of two prototypical sugar and aromatic substrates: glucose and benzoate. Glucose is the sugar monomer of the polymers cellulose and starch, which are common polysaccharides in plant matter; benzoate is a degradation product of lignin as well as a metabolic intermediate in the biodegradation of aromatic contaminants (Delmer et al., 2002; Michalska et al., 2012). Metabolic studies of *P. putida* KT2440 grown on benzoate or glucose as a sole carbon source have provided insights into the metabolic pathways involved in the catabolism of each substrate (Sudarsan et al., 2014; Kim et al., 2015; Nikel et al., 2015; Sudarsan et al., 2016; Sasnow et al., 2016). The initial catabolism of glucose and benzoate follows distinct paths before converging in the tricarboxylic acid

(TCA) cycle, which generates amino acid precursors and reducing equivalents for the cell (Fig. 1).

In *P. putida*, glucose enters the cytosol via two routes (del Castillo et al., 2007; Nikel et al., 2015; Sasnow et al., 2016) (Fig. 1). After entering the periplasm, glucose is either phosphorylated directly to glucose-6-phosphate (G6P) or oxidized first to gluconate in the periplasm followed by subsequent phosphorylation of gluconate to 6-phosphogluconate (6-PG) (del Castillo et al., 2007; Nikel et al., 2015; Sasnow et al., 2016) (Fig. 1). The G6P metabolite can be isomerized to fructose-6-phophate (F6P) or oxidized to 6-PG and generate a NADPH in the process. Since *P. putida* lacks the enzyme 6-phosphofructokinase for the conversion of F6P to fructose-1,6-bisphosphate (FBP) (Nelson et al., 2002), the forward Embden-Meyerof-Parnas (EMP) pathway is incomplete (Fig. 1). Therefore, glucose is primarily metabolized through the Entner-Doudoroff (ED) pathway, which splits 6-PG into two three-carbon compounds, glyceraldehyde 3-phosphate (GAP) and pyruvate (Fig. 1) (Wood, 1955; Wang et al., 1959; Castillo et al., 2007; Sudarsan et al., 2014; Nikel et al., 2015; Sasnow et al., 2016). Using the reverse EMP pathway, GAP and its isomer dihydroxyacetone-3-phosphate (DHAP) can combine to produce FBP, which can subsequently dephosphorylate to F6P (Fig. 1). In addition to the ED pathway, 6-PG is a precursor metabolite to the oxidative pentose phosphate (PP) pathway, which involves the decarboxylation of 6-PG to form eventually the PP metabolites ribose-5-phosphate (R5P) and xylulose-5-phosphate (Xu5P) (Fig. 1). This decarboxylation step also produces one mole of NADPH. On the other hand, the non-oxidative branch of the PP pathway yields PP metabolites by combining the glycolytic metabolites F6P and GAP (Fig. 1). The ED pathway-derived metabolites, GAP and pyruvate, eventually lead to the formation of acetyl coenzyme A (acetyl-CoA) via decarboxylation of pyruvate and the formation of oxaloacetate (OAA) via carboxylation of pyruvate or phosphoenolpyruvate (PEP) (Fig. 1). The combination of OAA and acetyl-CoA produces citrate, the first metabolite of the TCA cycle (Fig. 1).

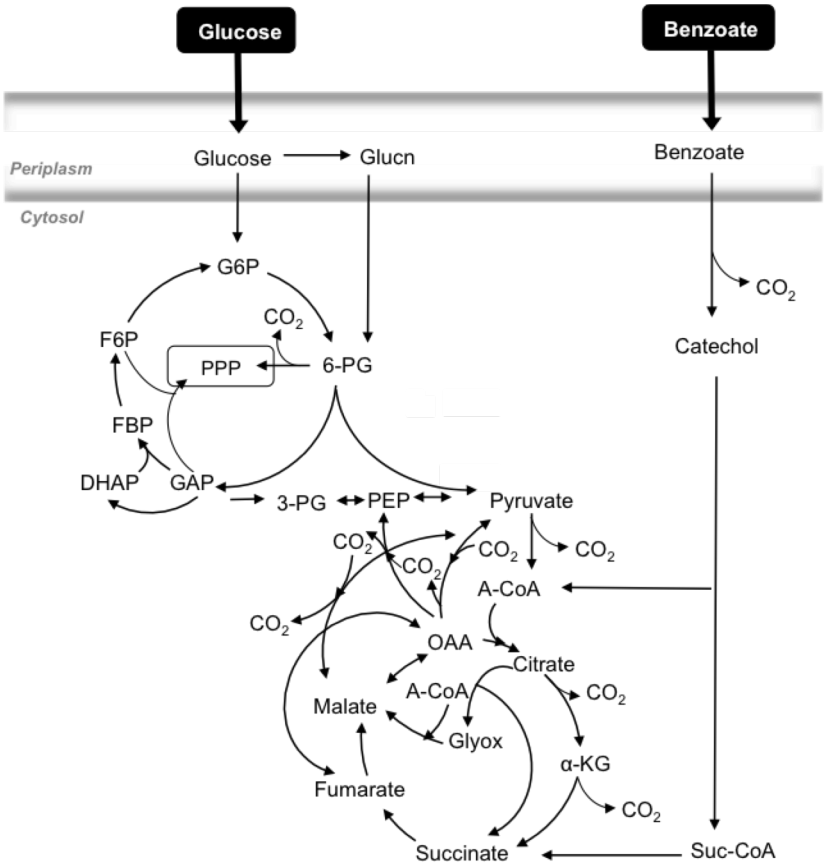

Figure 1: Metabolic routes for assimilation of glucose and benzoate in the Entner-Doudoroff (ED) pathway, the pentose phosphate (PP) pathway, the tricarboxylic acid (TCA) cycle and gluconeogenic and analeurotic pathways.
Abbreviations for metabolites: glucose-6-phosphate, G6P; 6-phosphate-gluconate; 6-PG; glyceraldehyde phosphate, GAP; dihydroxyacetone phosphate; DHAP; fructose-1,6-bisphosphate, FBP; fructose-6-phosphate, F6P; 3-phosphoglycerate, 3-PG; phosphoenolpyruvate, PEP; α-ketoglutarate, a-KG; oxaloacetate, OAA; glyoxylate, Glyox; acetyl-coenzyme A (acetyl-CoA), A-CoA; succinyl-coenzyme A (succinyl-CoA), Suc-CoA.

In regards to benzoate, this aromatic substrate is exclusively metabolized through the β-ketoadipate or *ortho*-cleavage (*ortho*) pathway in *P. putida* KT2440 wherein benzoate is eventually catabolized to acetyl-CoA and succinyl-CoA (Fig 1). In other *P. putida* strains, however, benzoate can be catabolized additionally via the *meta*-cleavage (*meta*) pathway, which yields acetyl-CoA and pyruvate (Worsey et al., 1975; Silva-Rocha et al., 2013; Silva-Rocha et al., 2014; Kim et al., 2015). The *meta* pathway is absent in *P. putida* KT2440 because it lacks the TOL plasmid that encodes for the *meta*-pathway (Nelson et al., 2002; Sudarsan et al., 2016). Both the acetyl-CoA and the succinyl-CoA produced through the

ortho-pathway in *P. putida* KT2440 feed into the TCA cycle for further metabolism (Loh and Chuna 2002; Sudarsan et al., 2016) (Fig. 1).

Previous studies have described the growth (del Castillo et al., 2007; Duuren et al., 2012; Sudarsan et al., 2014) and substrate consumption (Basu et al., 2006; del Castillo et al., 2007; Sudarsan et al., 2014; Karishma et al., 2016) of *P. putida* strains grown on glucose and an aromatic substrate. The growth rate of *P. putida* KT2440 (pWW0) was similar when fed on glucose alone, toluene alone, or a mixture (2.3 to 1 ratio) of glucose and toluene (del Castillo et al., 2007). Furthermore, a single exponential growth phase was reported for *P. putida* strains KT2440 (pWW0), KT2440-JD1, and KT2440 during feeding on growth media containing different ratios of, respectively, glucose to toluene (2.3 to 1) (del Castillo et al., 2007), glucose to benzoate (2.5 to1) (Duuren et al., 2012), and glucose to benzoate (10 to1) (Sudarsan et al., 2014). With respect to substrate consumption, measurements of extracellular substrate depletion implied that glucose and an aromatic substrate were consumed simultaneously in *P. putida* P8 (Cao et al., 2007), *P. putida* KT2440-JD1 (Duuren et al., 2012), *P. putida* KT2440 (Sudarsan et al., 2014), and *P. putida* mt-2 (Kim et al., 2015). However, a preference for aromatic compounds over glucose was reported in *P. putida* KT2440 (pWW0) (del Castillo et al., 2007) and *P. putida* KT2440 (Sudarsan et al., 2014). By contrast, *P. putida* CSV86 displayed a diauxic growth profile wherein glucose was preferentially used over the aromatic substrates during feeding on glucose and naphthalene (2.5 to 1), glucose and benzyl alcohol (2.5 to 1), or glucose and benzoate (2.5 to 1) (Basu et al., 2007; Karishma et al., 2016). Assimilation of stable isotope-labeled substrates in *P. putida* KT2440 (pWW0) indicated that carbons derived from both benzoate and glucose led to the production of amino acids from metabolite precursors downstream the ED pathway and from the TCA cycle (del Castillo et al., 2007). These previous results are in accordance with the proposal that the cells assimilated carbons from different substrates in a manner that optimizes biomass growth (del Castillo

et al., 2007). However, the cellular fluxes that channel these carbons through the different metabolic pathways remained to be fully elucidated.

In *P. putida*, the catabolite repression control (Crc) protein, which plays a role in regulating the assimilation of multiple substrates (Görke et al., 2008; Collier et al., 1996; Hester et al., 2000; Monero et al., 2009), has been shown specifically to regulate enzymes responsible for glucose metabolism in the ED pathway and reverse EMP pathway (Hester et al., 2000; Monero et al., 2009). Several metabolic changes have been reported for glucose metabolism in the presence of an aromatic substrate (Hester et al., 2000; del Castillo et al., 2007; Monero et al., 2009). Specifically, both ABC glucose transporters and glucokinase, the enzyme responsible for the phosphorylation of glucose to G6P, were downregulated in *P. putida* KT2440 (pWW0) in the presence of toluene compared to glucose-only growth condition (del Castillo et al., 2007). In addition, G6P dehydrogenase (G6PDH), which converts G6P to 6-PG, was also shown to be downregulated in the presence of aromatic substrates (naphthalene and benzyl alcohol) (Basu et al., 2006). However, the enzyme gluconokinase , which converts gluconate to 6-PG, was not affected by the presence of toluene (del Castillo et al., 2007). It remains unknown how the selective downregulation of enzymes involved in initial glucose catabolism influences the co-metabolism of both glucose and an aromatic substrate in downstream metabolic pathways in the central carbon metabolism.

The Crc protein is also known to regulate malate dehydrogenase (MALDH) (La Rosa et al., 2015). By catalyzing the decarboxylation of malate to pyruvate, MALDH is hypothesized to coordinate carbon overflow from the TCA cycle (La Rosa et al., 2015). Prior investigations of the metabolism of benzoate alone (Sudarsan et al., 2014; Sudarsan et al., 2016) or the co-metabolism of glucose and succinate (a downstream metabolite of benzoate catabolism) (La Rosa et al., 2015) in *P. putida* KT2440 have provided clues on the regulation of TCA cycle enzymes. For instance, the glyoxylate shunt, which produces malate and succinate while bypassing the two decarboxylation reactions downstream of

isocitrate in the canonical TCA cycle (Fig. 1), was shown to be activated in these two previous studies whereas this pathway was not active in *P. putida* KT2440 grown on glucose alone (Sudarsan et al., 2014; Nikel et al., 2015; Sasnow et al., 2016). The activation of the glyoxylate shunt in *P. aeruginosa* (Tiwari and Campbell, 1969), *E coli* (Walsh and Koshland, 1985), and *P. putida* (Nikel et al., 2014; Sudarsan et al. 2014; Sudarsan et al. 2016) was shown to be inversely correlated with the activity of isocitrate dehydrogenase (ICDH), which catalyzes the catabolism of isocitrate to α-KG in the TCA cycle. And, an *in silico* estimation of the flux from α-KG to succinate was minimal in *P. putida* grown on glucose and succinate (La Rosa et al., 2015) or on benzoate alone (Sudarsan et al., 2016), implying a decrease in α-KG dehydrogenase (alpha-KGDH) activity. Feedback inhibition of ICDH by succinyl-CoA, glyoxylate, and OAA was also reported in liver cells (Smith et al., 1973; Tretter et al., 2005) and *P. putida* (Nikel et al., 2014). Taken together, these previous reports of changes in enzymatic expressions implied a change in the routing of carbon within the TCA cycle during metabolism of an aromatic substrate. How these changes are manifested during co-metabolism of glucose and benzoate remain to be investigated.

In the present study, the metabolic network in the central carbon metabolism that directs the co-assimilation of the sugar glucose and the aromatic substrate benzoate was elucidated and the distribution of intracellular carbon fluxes in *P. putida* KT2440 was quantified. The central hypothesis is that the optimal metabolism for biomass growth on the substrate mixture will involve preferential flux of substrate-derived carbons through different metabolic pathways. Using a detailed metabolomics profiling approach involving liquid chromatography-mass spectrometry (LC-MS) and ^{13}C tracer experiments, we achieved the following three objectives: (1) determine the metabolic pathways involved in channeling the co-assimilation of glucose and benzoate in cellular metabolism, (2) determine the influence of benzoate on the connection between the TCA cycle and upstream metabolic pathways, and (3) quantify the cellular fluxes throughout the network of central carbon metabolism.

Intracellular metabolite labeling data revealed that benzoate-derived carbons populated the TCA-cycle, both benzoate and glucose were assimilated into metabolites downstream the ED pathway, and primarily glucose-derived carbons were channeled to the ED pathway, reverse EMP pathway, and PP pathway. Results from metabolic flux analysis (MFA) revealed that, in accordance with previously reported changes in enzyme activity, the influx of carbon from benzoate resulted in metabolic rerouting of the ED pathway, reverse EMP pathway, PP pathway, and the TCA cycle. These findings are informing a new framework both for accounting mixed-substrate metabolism in soil *Pseudomonas* species and for developing novel biotechnological applications, including bioremediation strategies or biofuel production.

CHAPTER 2: MATERIALS AND METHODS

2.1. Culturing conditions

Pseudomonas putida KT2440 was obtained from ATCC (American Type Culture Collection, Manassas, VA) as freeze-dried cultures. Cells were re-suspended and grown in liquid Luria-Bertani (LB) medium followed by plating on LB medium and storage at 4°C before use. For carbon source-specific growth, liquid cultures of *P. putida* KT2440 were grown in a 250-mL baffled flasks (cell suspension did not exceed one-tenth of the total flask volume) at 30°C in a G24 environmental incubator shaker (New Brunswick Scientific, Edison, NJ) shaken vigorously at 220 rpm (Sasnow et al., 2016). Flasks were covered with sponge caps to prevent contamination and allow gas exchange. The pH-adjusted (pH 7.0) and filter-sterilized (0.22 µm nylon; Waters Corporation, Massachusetts) growth medium contained the following: 20 mM K_2HPO_4, 5 mM NaH_2PO_4, 0.8 mM $MgSO_4 \cdot 7H_2O$, 37 mM NH_4Cl, 34 µM $CaCl_2 \cdot 2H_2O$, 30 µM $FeSO_4 \cdot 7H_2O$, 13 µM $CuSO_4 \cdot 5H_2O$, 0.97 µM H_3BO_3, 70 µM $ZnSO_4 \cdot 5H_2O$, 5.7 µM $MnSO_4 \cdot 5H_2O$, 0.21 µM $NiCl_2 \cdot 5H_2O$, and 1.2 µM $Na_2MoO_4 \cdot 5H_2O$. The total carbon-equivalent substrate concentration of 100 mM C was added as glucose or as a 50:50 glucose:benzoate mixture. Cell growth (three biological replicates) was monitored by measuring the optical density at 600 nm (OD_{600}) using an Agilent Cary UV-visible spectrophotometer (Santa Clara, California). As was done previously (Sasnow et al., 2016), the cells were transferred twice into fresh growth medium before conducting the experiments in order to ensure that cells were conditioned in their respective growth medium. The initial OD_{600} of the cells at each transfer was between 0.05 and 0.07. Cells were transferred during mid-exponential phase, between OD_{600} 0.5 and 1.0. An OD_{600} measurement was obtained every 60 min until stationary phase. Cell dry weight in grams (gCDW) were also determined following drying of 1-mL aliquots of exponentially-growing cell suspensions using a Labconco freeze-dryer (Kansas City, MO, USA). A conversion factor of 0.60 ± 0.42 $g_{CDW}\ L^{-1}$ per OD_{600} for the glucose:benzoate condition was used. This

value is in agreement with the value (0.58 ± 0.08 g_{CDW} L^{-1} per OD_{600}) previously determined for glucose-grown *P. putida* KT2440 (Sasnow et al., 2016).

2.2. Substrate consumption

To quantify the consumption of extracellular glucose and benzoate from the medium, samples (three biological replicates) were harvested throughout the growth of the cells. The extracellular samples were prepared for analysis by nuclear magnetic resonance (NMR) by mixing 250 µL of filtered sample (0.22 µm pore size nylon filters; Fisher Scientific, Pittsburgh, Pennsylvania) with 60 µL of 100% D_2O, 50 µL 2,2-dimethyl-2-silapentane-5-sulfonate (DSS) as a chemical shift reference compound, and 50 µL sodium-azide (NaN_3) as an antimicrobial agent. Samples were stored at 4°C until analysis time. The NMR samples were analyzed by ^1H NMR using a Varian Unity INOVA 600-MHz NMR spectrometer at 25°C (relaxation delay of 5 s, recording of 16 scans per sample, receiver gain of 32 dB) (Aristilde et al., 2015). Substrate consumption rates (in mmol $gCDW^{-1}$ h^{-1}) by exponentially-growing cells were determined by regression analysis.

2.3. Sampling for Intracellular and extracellular metabolite levels

To determine intracellular metabolic pseudo steady-state conditions, we obtained intracellular metabolite levels across the growth phases of the cultures (three biological replicates) grown on glucose (100 mM C) or glucose:benzoate mixture (50:50 at a total 100 mM C). Cell suspensions (3 mL) were collected at four OD_{600} values (0.5, 1.0, 2.0, 4.5). The suspensions were filtered and the cell-containing filters were immediately quenched with a cold (4°C) 2-mL solution of methanol:acetonitrile:water (40:40:20). Solutions with the lysed cells were subsequently filter-centrifuged (Sigma Aldrich Spin-X 0.22 µm filters). Aliquots of the supernatants were dried under nitrogen gas and re-suspended in ultrapure LC-MS water (Fisher Scientific, Pittsburgh, Pennsylvania) before analysis via LC-MS (see *Section 2.5*). Metabolite levels were normalized to biomass quantity at the time of sampling.

To monitor metabolite excretion rates, metabolites in the extracellular medium were quantified during exponential phase. Aliquots (250 µL) of the cell suspensions were collected for each of the three biological replicates followed by centrifugation (21,130 *g* for 5 min) and filtration (0.22 µm pore size nylon filters) to remove cell particulates. The supernatants were prepared for LC-MS analysis as described above. After drying, re-suspension in LC-MS grade ultrapure water was diluted (by 5x) before LC-MS analysis (see *Section 2.5*). Metabolite excretion rates (µmol $gCDW^{-1}$ h^{-1}) were determined by regression analysis.

2.4. Long-term and kinetic intracellular metabolite labeling

For long-term intracellular labeling, culturing conditions were as described above with two transfers of cultures (three biological replicates) into fresh growth medium with labeled substrates purchased from Cambridge Isotopes (Tewskbury, MA, USA) or Omicron Biochemicals (South Bend, IN, USA). The labeled substrates were the following: [U-$^{13}C_6$]-glucose, [U-$^{13}C_6$]-glucose with unlabeled glucose, [1,5,6-$^{13}C_3$]-glucose, or [1,5,6-$^{13}C_3$]-glucose with unlabeled benzoate. At two times points during mid-exponential phase (OD_{600} of 0.5 and 1.0), the cells (3 mL) were filtered, quenched, and prepared as described above (see *Section 2.3*) and subsequently analyzed by LC-MS (see *Section 2.5*).

To capture the influence of benzoate on *in vivo* metabolic enzyme activity in glucose-acclimated cells, we carried out a kinetic metabolic flux experiment. Cells were first grown in a medium recipe, as described above (see *Section 2.1*), which contained fully labeled [U-$^{13}C_6$]-glucose (200 mM C). Cells were transferred twice as described in *Section 2.1* into this labeled growth medium in order to ensure near-complete isotopic labeling of intracellular metabolites. At early exponential phase after the second transfer, aliquots (3 mL) of the cell suspensions were filtered and the cell-containing filters were transferred to a plate with agar-solidified growth medium with [U-$^{13}C_6$]-glucose. Once the cells growing on the plates

had reached mid-exponential phase (~OD_{600} 0.5—1.0), the cell-containing filters were subsequently transferred to plates that contained unlabeled benzoate (200 mM C)—see Aristilde (2016) for details on how to monitor cell growth on the plates. At specific time points (15 sec, 30 sec, 1 min, 2 min, 5 min, 30 min, 60 min, 120 min) following the isotopic switch, the cell-containing filters were quenched and prepared as described above (see *Section 2.3*). The metabolite extracts were analyzed via LC-MS (see *Section 2.5*).

2.5. Metabolomics analysis via LC-MS

Metabolite extracts obtained as described in *Sections 2.3* and *2.4* were analyzed by reversed-phase ion-pairing liquid chromatography using ultra-high performance liquid chromatography (UHPLC; Thermo Scientific DionexUltiMate 3000) coupled with high-resolution/accurate-mass mass spectrometer (MS) (Thermo Scientific Q Exactive quadrupole-Orbitrap hybrid MS) with electrospray ionization (ESI) operated in negative mode. Solvent A contained 97:3 (v/v) LC-MS grade H_2O: methanol with acetic acid (15 mM) and tributylamine (10 mM). Solvent B contained 100% methanol. The flow rate was 180 µL min^{-1} during the entire sample run (25 min). The solvent gradient with respect to solvent A was the following: 0 min, 100%; 2.5 min, 100%; 5 min, 80%; 7.5 min, 80%; 10 min, 45%; 12 min, 45%; 14 min, 5%; 17 min, 5%; 18 min, 0%; 25 min, 0% was run. An injection sample of 10 µL was used and the column temperature was set to 25°C (Lu et al., 2010). A Waters Acquity UPLC BEH C_{18} column (1.7µm with column size 2.1 x 100mm) (Waters Corporation, Massachusetts, USA) was used. The following metabolites were monitored: G6P, gluconate, F6P, R5P, Xu5P, S7P, FBP, DHAP, 3-phosphoglycerate (3-PG), phosphoenolpyruvate (PEP), pyruvate, citrate, α-ketoglutarate (α-KG), succinate, fumarate, malate, aspartate, glutamate, glutamine (Gln). As done in previous metabolomics studies, oxaloacetate (OAA) was taken to be the same as the aspartate labeling because aspartate

is an amino acid directly synthesized from OAA (Amador-Noguez et al., 2010; Sasnow et al., 2016). All metabolite identification and isotopic enrichment were determined using the Metabolomics Analysis and Visualization Engine (MAVEN) software package (Clasquin et al., 2012). The ^{13}C-labeled fractions were corrected for natural ^{13}C abundance.

2.6. Metabolic flux quantitation

Using the software 13CFLUX2 (Weitzel et al. 2012), a MFA of the central carbon metabolism was performed using experimental data (average ± standard deviation) as constraints. The experimental data were obtained with cells (three biological replicates) at metabolic pseudo steady-state, which was confirmed to occur in the exponentially-growing cells. The MFA was constrained on carbon-equivalent carbon consumption and metabolite excretion rates, long-term labeling of intracellular metabolites following growth on [1,5,6-$^{13}C_3$]-glucose alone or with unlabeled benzoate, and effluxes of metabolite-derived carbons toward biomass production (Sasnow et al., 2016). Using the biomass growth rates determined experimentally and published biomass composition of *P. putida* KT2440 (Van Durren et al., 2013), biomass conversion rates were calculated for metabolite precursors to amino acids and nucleotides. The ^{13}C-labeling data used in the MFA were for the following metabolites: gluconate, G6P, F6P, R5P, Xu5P, S7P FBP, DHAP, 3-PG, PEP, pyruvate, citrate, α-KG, fumarate, and aspartate for OAA. Initial flux values were set based on published values (Sasnow et al., 2016; Nikel et al., 2015; La Rosa et al., 2015) and subsequently optimized based on the aforementioned experimentally-obtained data. The quality of the fit to experimental data was measured by calculating residuals based on comparisons of model-estimated metabolite labeling patterns to the measured values (Zamboni et al., 2009; Sasnow et al., 2016).

CHAPTER 3: RESULTS AND DISSCUSION

3.1 Growth phenotype and substrate consumption

The specific growth rate and extracellular substrate depletion rate were determined with exponentially-growing *P. putida* KT2440 cells grown on a 1:1 glucose:benzoate mixture with a total of 100 mM C (Fig. 2A and 2B; Appendix A, Fig. A1 and A2). For comparisons, growth experiments were also conducted with glucose alone at the same total carbon-equivalent concentration (Fig 2A). The specific growth rate of glucose-grown cells, 0.68 ± 0.09 h^{-1} (Fig. 2A), was in close agreement with previously-reported values obtained with glucose-grown *P. putida* KT2440, 0.56 ± 0.02 h^{-1} (del Castillo et al., 2007), and 0.60 ± 0.04 h^{-1} (Sasnow et al., 2016), and glucose-grown *P. fluorescens* 52-1C, 0.65 ± 0.05 h^{-1} (Fuhrer et al., 2005). For *P. putida* KT2440 cells grown on the 1:1 glucose:benzoate mixture, we obtained a growth rate of 0.93 ± 0.10 h^{-1} (Fig. 2A). A previous study with *P. putida* KT2440 (pWW0) grown on a 2.3 to glucose:toluene mixture reported a comparable growth rate, 0.73 ± 0.07 h^{-1} (del Castillo et al. 2007). These similar growth rates at different ratios of glucose to an aromatic substrate implied that different strains of *P. putida* are capable of incorporating the different carbons to maintain optimal biomass growth.

Accordingly, we obtained comparable values for the total carbon consumption rates for *P. putida* KT2440 cells grown on glucose alone or with benzoate (Fig. 2B). For the glucose-only growth condition, the rate of glucose consumption was 48.5 ± 13.8 mmol C $gCDW^{-1}$ h^{-1} or 8.09 ± 2.3 mmol glucose $gCDW^{-1}$ h^{-1} (Fig. 2B), which was consistent with a published value for glucose-grown *P. putida* KT2440, 6.14 ± 0.04 mmol glucose $gCDW^{-1}$ h^{-1}, (Nikel et al., 2015) but was greater than two other published values of glucose-grown *P. putida* KT2440, 4.79 ± 0.39 mmol glucose $gCDW^{-1}$ h^{-1} (del Castillo et al., 2007) and 4.71 ± 0.30 mmol glucose $gCDW^{-1}$ h^{-1} (Sasnow et al., 2016). During growth on the glucose:benzoate mixture, the carbon-equivalent consumption rate of glucose and benzoate was respectively 19.8 ± 4.4 mmol C $gCDW^{-1}$ h^{-1} and 27.2 ± 8.1 mmol C $gCDW^{-1}$ h^{-1} (Fig. 2B). Thus, the total

carbon consumption rate from the substrate mixture, 47.0 ± 11.2 mmol C $gCDW^{-1}$ h^{-1}, was similar to the carbon-equivalent consumption rate of glucose alone (48.5 ± 13.8 mmol C $gCDW^{-1}$ h^{-1}).

It is widely accepted that *Pseudomonas* spp. prefer organic acids and aromatic compounds over glucose (MacGregor et al., 1992; Hester et al., 2000; Basu et al., 2006; Sudarsan et al., 2014; La Rosa et al., 2015; Karishma et al., 2016). However, the growth medium in previous studies often contain a higher amount of glucose than the other substrate. Morevoer, there have been cases in which *Pseudomonas* spp. (*P. aeruginoasa* PP4 and *Pseudomonas* sp. C5pp) have been shown to prefer glucose over aromatics (Karishma et al., 2016). Our growth and substrate depletion imply that at similar carbon-equivalent amounts, glucose and benzoate support biomass growth rate comparable to

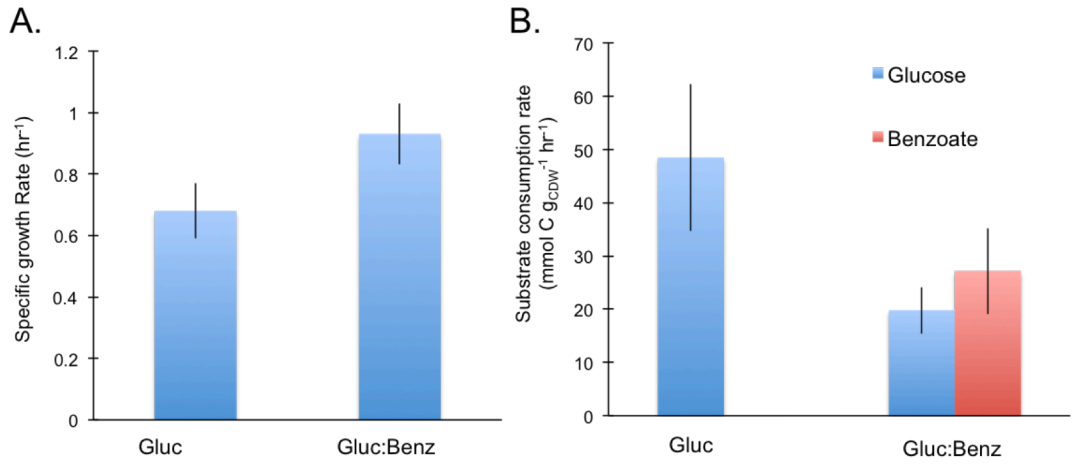

Figure 2: Growth rate (A) and substrate consumption rate (B) of *P. putida* KT2440 exponentially-growing on Glucose (Gluc) (100 mM C) or a 50:50 mixture of Glucose:Benzaote (Gluc:Benz) (50mM C each). Data (average ± standard deviation) are from biological replicates (*n* = 3).

cells grown on glucose alone. We performed a series of experiments with different labeling schemes to elucidate the intracellular metabolism in *P. putida* KT2440 that channels the co-utilization of both sugar and aromatic substrates to support this optimal biomass growth.

3.2. Partitioning of assimilated substrates in the metabolic network structure

Using ^{13}C tracer experiments, we investigated the investment of assimilated glucose and benzoate into the intracellular metabolites in the ED pathway, reverse EMP pathway, PP pathway, and the TCA cycle (Fig. 3, 4, and 5). First, we monitored metabolite labeling in *P. putida* KT2440 cells grown on [U-$^{13}C_6$]-glucose with unlabeled benzoate (Appendix A, Fig. A3). To ascertain that the isotopic enrichment was at steady-state, the ^{13}C-labeling patterns of metabolites extracted from cells were compared at two different times (OD_{600} of 0.5 and 1.0) during the exponential growth phase (Appendix A, Fig. A4 and A5). For comparison, metabolite ^{13}C-labeling patterns were also obtained during *P. putida* KT2440 growth on [U-$^{13}C_6$]-glucose alone and these patterns indicated, as expected, near complete isotopic enrichment in the labeling of all the metabolites (Appendix A, Fig. A3). For cells grown on the glucose:benzoate mixture, the data revealed that *P. putida* KT2440 partitioned carbon derived from benzoate to the TCA cycle and carbon derived from glucose to the ED pathway, reverse EMP pathway, and PP pathway (Appendix A, Fig. A3). Metabolites that were downstream of the ED pathway consisted of carbon from both glucose and benzoate pathway (Appendix A, Fig. A3).

To elucidate in more details the selective partitioning of both glucose- and benzoate-derived carbons in specific pathways in the metabolic network, we performed additional long-term isotopic enrichment of intracellular metabolites by growing cells on [1,5,6-$^{13}C_3$]-glucose alone or with unlabeled benzoate (Fig. 3, 4, and 5). First, we established the network of carbon flow for initial glucose catabolism, the ED pathway, the reverse EMP pathway, and the PP pathway (Fig. 3). In accordance with the oxidation of [1,5,6-$^{13}C_3$]-glucose in the periplasm, gluconate was nearly completely triply ^{13}C-labeled in the absence (99.1 ± 0.0%) and presence of benzoate (97.1 ± 0.6%) (Fig. 3). Both the phosphorylated metabolites in glucose catabolism, G6P and 6-PG, were primarily triply ^{13}C-labeled, respectively 71.8 ± 4.1% and 87.6 ± 0.1% in the absence of benzoate and, in presence of

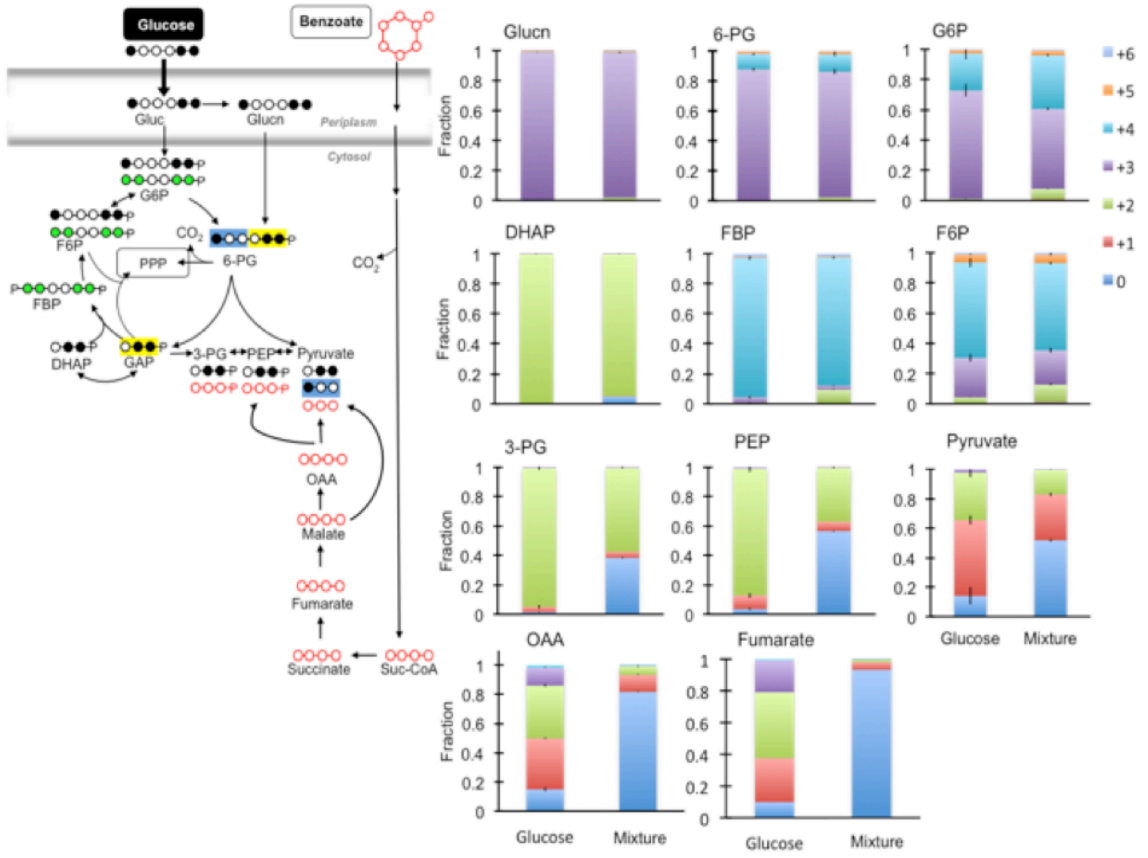

Figure 3: Cellular network for the co-metabolism of glucose and benzoate in *P. putida* KT2440. Steady-state labeling of intracellular metabolites in the ED and EMP pathways during growth on [1,5,6 $^{13}C_3$]-glucose alone (Glucose) or with unlabeled benzoate (Mixture). Data (average ± standard deviation) are from biological replicates (n = 3). Metabolite abbreviations are the same as in Fig. 1.

benzoate, 52.8 ± 4.1% and 84.0 ± 0.1% (Fig. 3). Since both G6P and gluconate are precursors to 6-PG, the higher enrichment in triply ^{13}C-labeled 6-PG compared to G6P implied greater flux of gluconate than from G6P for the biosynthesis of 6-PG (Fig. 3). Through the ED pathway, triply ^{13}C-labeled 6-PG splits into singly ^{13}C-labeled pyruvate and doubly ^{13}C-labeled GAP (Fig. 3). Consistent with the occurrence of the ED pathway, we obtained singly ^{13}C-labeled forms of pyruvate (51.4 ± 3.2% in the absence of benzoate and 31.2 ± 1.2% in the presence of benzoate) and doubly ^{13}C-labeled DHAP, an isomer of GAP (99.3 ± 0.3% and 94.7 ± 0.3% respectively in the absence and presence of benzoate) (Fig.

3). In addition to singly ^{13}C-labeled form, the presence of doubly ^{13}C-labeled pyruvate both in the absence (32.3 ± 3.4%) and presence of benzoate (16.6 ± 0.4%) highlighted the participation of both the ED pathway and the metabolites downstream of GAP to form pyruvate. In fact, doubly ^{13}C-labeled forms of 3-PG and PEP were, respectively 94.6 ± 1.5% and 86.3 ± 2.4% in the absence of benzoate and respectively 57.2 ± 0.6% and 36.9 ± 0.5% in the presence of benzoate (Fig. 3). The decrease in doubly ^{13}C-labeled fraction of 3-PG and PEP during growth on the glucose:benzoate mixture was accompanied by an increase in nonlabeled fraction in 3-PG (38.4 ± 0.1%) and PEP (56.7 ± 0.0%) (Fig. 3). In a similar manner, the nonlabeled fraction in pyruvate (51.8 ± 1.0%) explained why the singly ^{13}C-labeled pyruvate from the ED pathway, as reported above, was less in cells grown on the mixture compared to growth on glucose alone (Fig. 3). Therefore, the data showed that nonlabeled benzoate-derived carbons were incorporated into 3-PG, PEP, and pyruvate. These results agreed with a previous report of the presence of toluene-derived carbons in serine, an amino acid derived from 3-PG, when *P. putida* KT2440 (pWW0) was grown on both toluene and glucose (del Castillo et al., 2007).

However, there was only a small fraction of nonlabeled DHAP (5.2 ± 0.2%) during growth on the glucose:benzoate mixture, , indicating that the incorporation of benzoate carbons above 3-PG was insignificant. However, despite the lack of benzoate-derived carbons into the reverse EMP pathway and PP pathway, there were noticeable changes in the routing of carbons in both pathways during growth on the mixture. Through the reverse EMP pathway, the ED pathway-generated doubly ^{13}C-labeled GAP combines with its isomer DHAP to form quadruply ^{13}C-labeled FBP, which subsequently dephosphorylates to produce quadruply ^{13}C-labeled F6P (Fig. 3). In accordance with the flow of carbon through the reverse EMP pathway, I obtained quadruply ^{13}C-labeled forms of both FBP and F6P during growth on glucose alone (respectively, 92.7 ± 1.2% and 63.1 ± 3.0%) and during growth on glucose and benzoate (respectively, 85.3 ± 0.1% and 57.8 ± 1.0%) (Fig. 3). The formation of G6P can result either from the isomerization of F6P or from the

phosphorylation of glucose whereby the first reaction would generate quadruply ^{13}C-labeled G6P (in addition to other forms) and the latter reaction would provide only triply ^{13}C-labeled G6P (Fig. 3). We found that G6P in cells grown on the mixture had a larger fraction of quadruply ^{13}C-labeled fraction (35.6 ± 0.7%) and a smaller fraction triply ^{13}C-labeled fraction of G6P (52.8 ± 4.1%) compared to cells grown on glucose alone (respectively, 24.5 ± 3.9% and 71.8 ± 4.1%) (Fig 3). These results thus implied a greater recycling flux of assimilated glucose through the reverse EMP pathway in the presence of benzoate. On the other hand, the fractions of triply and quadruply labeled ^{13}C-labeled forms of 6-PG were nearly identical during growth on glucose alone (87.6 ± 0.1% and 10.4 ± 1.0%) and on the glucose:benzoate mixture (84.3 ± 0.9% and 11.6 ± 1.3%) (Fig. 3). In order to achieve these similar labeling fractions in 6-PG under both growth conditions given the different labeling pattern of G6P, we hypothesized that *P. putida* KT2440 decreased the flux from G6P to 6-PG when grown on the glucose:benzoate mixture. These hypothetical changes in fluxes through the reverse EMP pathway will be addressed further via MFA modeling in the next section (see *Section* 3.3).

With regards to the PP pathway, the labeling patterns of Xu5P and R5P indicated the participation of both the oxidative and nonoxidative routes of the PP pathway (Fig. 4). Through the oxidative pathway, a decarboxylation reaction would generate doubly ^{13}C-labeled pentose-phosphate metabolites from triply ^{13}C-labeled 6-PG (Fig. 4). During growth on glucose alone, we measured the doubly ^{13}C-labeled forms of R5P and Xu5P at, respectively, 28.2 ± 1.3% and 26.3 ± 2.1%; the corresponding values during growth on the mixture were 33.6 ± 2.9% and 33.6 ± 2.9% (Fig. 4). Given the greater than 80% fraction of 6-PG in triply ^{13}C-labeld forms, the relatively low fraction of doubly ^{13}C-labeled R5P and Xu5P indicated that the oxidative PP pathway was not the major biosynthetic route for these PP metabolites under both growth conditions, in agreement with previously reported fluxes for glucose-grown *P. putida* KT2440 (Sasnow et al., 2016), Through the nonoxidative pathway, the aforementioned labeling patterns of F6P and GAP combine through a series of

reactions to generate eventually quadruply ^{13}C-labeled Xu5P and R5P which were measured to be, respectively, 60.1 ± 2.0% and 55.4 ± 3.8% during growth on glucose alone and 55.2 ± 3.8% and 56.1 ± 3.7% during growth on the substrate mixture (Fig. 4). These labeling patterns of these PP intermediates thus highlighted a near two-to-one relative involvement of the nonoxidative PP pathway versus the oxidative PP pathway to generate pentose phosphates during growth on both conditions (Fig. 4).

However, the ^{13}C-labeling pattern of S7P, another intermediate in the PP pathway, indicated a different routing of carbons within the nonoxidative PP pathway for each condition (Fig 4). As illustrated in Fig 4, the two ways of generating S7P are via the transketolase reaction that combines the first two carbons from Xu5P with the 5-carbon R5P

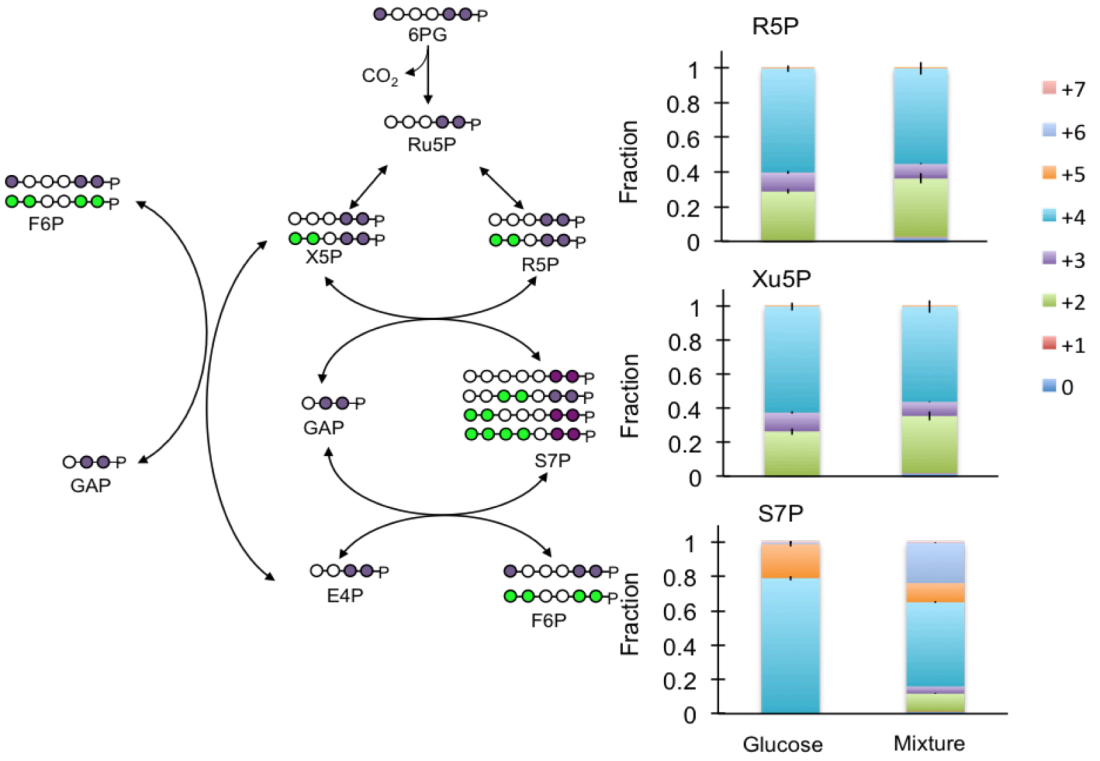

Figure 4: Cellular network for the co-metabolism of glucose and benzoate in *P. putida* KT2440. Steady-state labeling of intracellular metabolites in the PP pathway during growth on [1,5,6 $^{13}C_3$]-glucose alone (Glucose) or with unlabeled benzoate (Mixture). Data (average ± standard deviation) are from biological replicates (n = 3). Metabolite abbreviations are the same as in Fig. 1.

or the transaldolase reaction that combines the first three carbons from F6P with the 4-carbon E4P. Based on the labeling patterns of the different metabolites, the transketolase reaction would yield primarily quadruply and sextuply ^{13}C-labeled forms of S7P whereas the transaldolase reaction would yield primarily quadruply ^{13}C-labeled S7P as well as some quintuply ^{13}C-labeled S7P—the backward flux of the transaldolase reaction would generate triply ^{13}C-labeled E4P that would produce the quintuply ^{13}C-labeled S7P when combined with F6P in the forward flux (Fig. 4). When fed on the glucose alone, the cells generated two main labeled forms of S7P: primarily quadruply ^{13}C-labeled (79.1 ± 1.4%) and quintuply ^{13}C-labeled (19.8 ± 1.4%) (Fig. 4). On the other hand, the cells fed on the glucose:benzoate mixture had completely different labeling patterns: primarily quadruply ^{13}C-labeled S7P (49.1 ± 4.0%) and sextuply ^{13}C-labeled S7P (23.6 ± 2.8%), and some other minor labeling forms (Fig. 4). Therefore, S7P was primarily made from the transaldolase reaction during growth on glucose alone but primarily from the transketolase reaction downstream of the oxidative PP pathway during growth on the mixture. The relative fluxes of these two reactions will be determined using MFA and discussed in the following section (Fig. 4) (see *Section* 3.3).

Next, we monitored the assimilation of carbons through the TCA cycle. When cells were grown on glucose alone, the ^{13}C-labeling patterns of metabolites were consistent with the canonical routing of carbons through the TCA cycle (Fig 5). During feeding on glucose alone, anapleurotic reactions through the carboxylation of pyruvate and PEP (incorporating either nonlabeled or singly ^{13}C-laeled carbon dioxide) would generate the same labeling patterns already described for PEP and pyruvate without or with one extra ^{13}C carbon (Fig. 5). Accordingly, OAA (via aspartate) was determined to be 14.8 ± 1.0% nonlabeled, 35.0 ± 0.4% singly, 36.2 ± 0.8% doubly, 12.4 ± 0.3% triply (Fig. 5). Decarboxylation of pyruvate during feeding on glucose alone would produce nonlabeled acetyl-CoA (from both nonlabeled and singly and ^{13}C-labeled pyruvate) and doubly ^{13}C-labeled acetyl-CoA (from doubly^{13}C-labeled pyruvate) (Fig. 5). Consistent with the combination of acetyl-CoA with

OAA, the labeling pattern of citrate (7.8 ± 0.5% nonlabeled, 23.9 ± 0.6% singly, 31.9 ± 0.2% doubly, 21.7 ± 0.5% triply, and 11.4 ± 0.4% quadruply ^{13}C-labeled) (Fig. 5). Subsequent decarboxylation of citrate produced α-KG (21.0 ± 0.8 % nonlabeled, 25.6 ± 1.0% singly, 27.1 ± 0.9% doubly, 17.1 ± 0.8% triply, and 7.0 ± 0.5% quadruply ^{13}C-labeled) (Fig. 5). Fumarate labeling (9.9 ± 5.0% nonlabeled, 27.7 ± 3.0% singly, 41.5 ± 2.9% doubly, 20.1 ± 2.2% triply. and 0.7 ± 0.5% quadruply ^{13}C-labeled) was consistent with the occurrence of another decarboxylation step between α-KG to produce succinate, the direct precursor to fumarate (Fig. 5).

In cells grown on the glucose:benzoate mixture, it was clear from the aforementioned nonlabeled fractions of PEP and pyruvate that there was gluconeogenic flux from TCA cycle metabolites during growth on the glucose:benzoate mixture (Fig. 3). The influx of nonlabeled carbons from benzoate catabolism via the *ortho* pathway dominated the TCA cycle metabolites (Fig. 5). The *ortho* pathway would generate nonlabeled acetyl moiety in acetyl-CoA and nonlabeled succinyl moiety in succinyl-CoA (Fig. 1). Notably, the similarity between the labeling patterns of citrate and those in OAA indicated that the acetyl moiety in acetyl-CoA originated almost exclusively from nonlabeled benzoate (Fig. 1 and Fig. 5). Citrate (78.5 ± 0.4% nonlabeled, 12.2 ± 0.6% singly, and 8.1 ± 0.2% doubly ^{13}C-labeled) was produced from combining the nonlabeled acetyl moiety with OAA (81.7 ± 0.3% nonlabeled, 11.6 ± 0.4% singly, and 6.0 ± 0.3% doubly ^{13}C-labeled) (Fig. 5). The remaining TCA cycle metabolites measured were primarily nonlabeled, nonlabeled α-KG at 82.9 ± 0.8% and nonlabeled fumarate at 93.2 ± 2.0% (Fig. 5). The influx of nonlabeled succinate from benzoate increased the nonlabeled fraction in fumarate by up to 10.3% compared to nonlabeled α-KG (Fig. 5).

As discussed in detail above, tracking the ^{13}C-labeling patterns of the intracellular metabolites allowed us to map out the metabolic network in cells that are metabolizing glucose alone versus both glucose and benzoate (Fig. 3, 4, and 5). Thereafter, we applied a

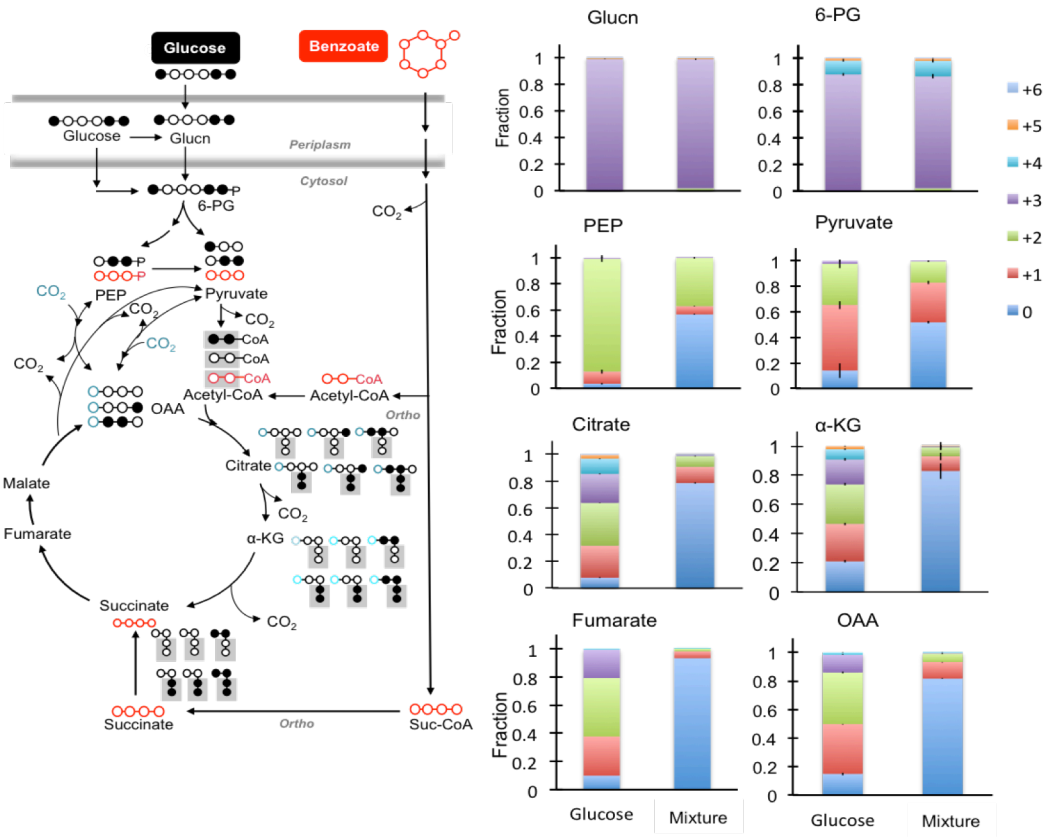

Figure 5: Cellular network for the co-metabolism of glucose and benzoate in *P. putida* KT2440. Steady-state labeling of intracellular metabolites in the TCA cycle during growth on [1,5,6 $^{13}C_3$]-glucose alone (Glucose) or with unlabeled benzoate (Mixture). Data (average ± standard deviation) are from biological replicates (n = 3). Metabolite abbreviations are the same as in Fig. 1.

MFA approach to quantify the carbon fluxes through the series of metabolic reactions in the cellular network.

3.3. Quantitative analysis of metabolic network fluxes

Fluxes through a total of 33 reactions were quantified in the metabolic network, which was constructed based on the results from the previous section and prior MFA studies on *P. putida* (Fuhrer et al., 2005; del Castillo et al., 2007; Puckalka et al., 2008; Blank et al., 2008; Sudarsan et al., 2014; Nikel et al., 2015; La Rosa et al., 2015; Sasnow et al., 2016; Sudarsan et al., 2016). In addition to the steady-state ^{13}C-labeling experiments with [1,5,6

$^{13}C_3$]-glucose, the MFA was constrained using experimentally-determined substrate consumption rates, metabolite excretion rates, and biomass growth. The agreement between model-estimated and experimentally-determined labeling patterns demonstrated the good quality of the optimization fits for modeling the carbon metabolism in cells grown on glucose-alone or together with benzoate (Appendix A, Fig. A6 and A7, respectively).

The normalized reactions rates (ratio of metabolic reaction rates over the composite substrate uptake rate) were determined (Fig. 6; Appendix A, Table A1). The rates for the glucose-only model were in agreement with previously reported values (Sasnow et al., 2016) (Appendix A, Table A1); Sasnow et al. (2016) showed that their MFA results were in agreement with Fuhrer et al., 2005; del Castillo et al., 2007; Blank et al., 2008; Sudarsan et al., 2014). We evaluated the sensitivity of the MFA results for the co-metabolism of glucose and benzoate to changes in carbon investment into biomass (either 100% less or 50% greater than the reference value). The results of the sensitivity analysis indicated that the substantial changes in biomass investment did not alter the metabolic reaction rates outside of their error imprecision of one to two standard deviation values (Appendix A, Fig. A8). There are no prior MFA performed for *P. putida* KT2440 grown on a glucose and an aromatic substrate with which to compare our MFA results for the co-metabolism of glucose and benzoate. I evaluated the results in relation to compared the MFA results for metabolism of the glucose:benzoate mixture with previous flux balance analysis (FBA) models in which *P. putida* KT2440 was grown on glucose and succinate (La Rosa et al., 2015) or on benzoate alone (Sudarsan et al. 2016). We note that, in these prior FBA models, metabolic fluxes were estimated by assigning objective functions based on biomass growth. By contrast, the MFA model presented here employed the explicit ^{13}C-labeling of metabolites to discriminate flux patterns through central carbon metabolism.

In the MFA model for glucose:benzoate co-metabolism, the normalized rates for glucose uptake (40.6 ± 4.6%) and benzoate uptake (59.4 ± 0.2%) were consistent with the relative fraction of the experimentally-determined values for substrate consumption (42.1 ±

9.4% and 57.9 ± 17.2%, respectively) (Fig. 6; Appendix A, Table S1). Interestingly, for both growth on glucose alone or in the presence of benzoate, the MFA revealed similar fractional ratio of the total glucose uptake rate that was subjected to oxidation to gluconate versus direct entry into the cytosol through phosphorylation to G6P. Specifically, for the fractional rate of glucose uptake converted to gluconate, 80.6 ± 0.0% was determined for glucose alone and 82.3 ± 9.9% when glucose was present with benzoate; and, for the fractional amount of glucose uptake towards G6P, 16.0. ± 6.5% when cells were grown on glucose alone and 17.7 ± 1.5% during growth on the mixture with benzoate (Fig. 6; Appendix A, Table S1). In cells grown on the glucose:benzoate mixture, a smaller fraction of total assimilated carbon was cycled through the ED pathway and reverse EMP pathway, compared to the glucose-only model (Fig. 6). This was indicated by the decreased fluxes from 6-PG to pyruvate and GAP (38.2 ± 4.0%), GAP to DHAP (17.5 ± 1.6%), DHAP and GAP to FBP (6.1 ± 0.2%), FBP to F6P (9.4 ± 4.2%) and F6P to G6P (4.3 ± 0.6%) when cells were grown on the glucose:benzoate mixture compared to cells grown on glucose alone (110 ± 5.4%, 28.6 ± 2.0%, 25.5 ± 1.4%, 25.5 ± 1.4%, and 14.2 ± 1.7%, respectively) (Fig. 6). Despite the decrease in carbon fluxes through the ED pathway and reverse EMP pathway, investment of carbon into the PP pathway via both the oxidative and nonoxidative routes was maintained when cells where grown on the glucose:benzoate mixture (2.2 ± 0.2% and 4.5 ± 2.3%, respectively) or glucose alone (2.7 ± 0.4% and 7.4 ± 0.0%, respectively), (Fig. 6). Thus, *P. putida* KT2440 maintained the same flux towards metabolite precursors for ribonucleotide synthesis irrespective of significant changes in carbon fluxes through the ED pathway and reverse EMP pathway.

When cells were grown on the glucose:benzoate mixture, the MFA model indicated that G6PDH activity was decreased. When cells were grown on glucose alone, the fractional flux to gluconate (79.3 ± 1.9%) and G6P (33.2 ± 3.9%) to 6-PG was higher than when grown on the glucose:benzoate mixture (31.1 ± 4.2% and 9.2 ± 0.2%, respectively) (Fig. 6). In the glucose-grown cells, 6-PG was derived primarily from gluconate (70.5 ± 1.7%) and

secondarily from G6P (29.5 ± 3.5%) (Fig. 6). These results corroborated previous metabolic flux studies in which 6-PG was primarily derived from gluconate when *P. putida* KT2440 was grown on glucose alone (Nikel et al., 2015; Sasnow et al., 2016) (Table 3). When cells were grown on the glucose:benzoate mixture, the fraction derived from G6P (22.8 ± 0.0%) decreased 7% on average (Fig. 6). In a previous study, Basu et al. (2006) reported that the presence of aromatic substrates (naphthalene and benzyl alcohol) suppressed G6PDH activity in *P. putida* CSV86, even if glucose is also present in the growth medium (Basu et al., 2006). Furthermore, the Crc protein, which has been shown to regulate the co-utilization of mixed substrates in *P. putida* KT2440 (La Rosa et al., 2015), was also reported to

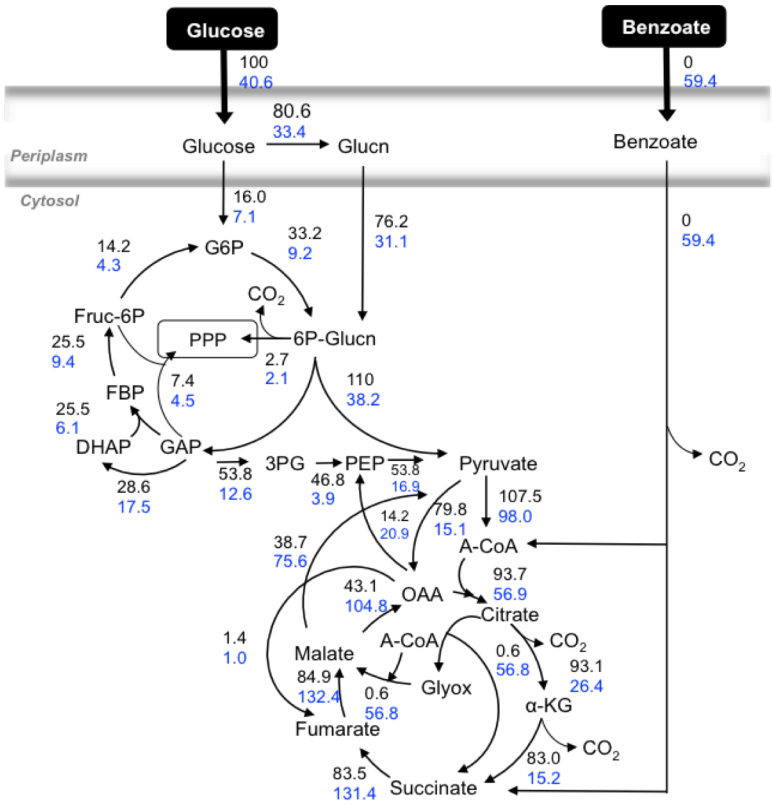

Figure 6: Quantitative analysis of metabolic network fluxes during growth on [1,5,6 $^{13}C_3$]-glucose alone (Black) or with unlabeled benzoate (Blue). Data (average) are from biological replicates (*n* = 2). Metabolite abbreviations are the same as in Fig. 1.

regulate G6PDH activity in *P. putida* (Hester et al., 2000). A previous study indicated that the activity of gluconokinase, which catalyzes the conversion of gluconate to 6-PG, was not

altered when *P. putida* KT2440 (pWW0) was grown on a glucose:toluene (2.3:1) mixture compared to glucose alone (del Castillo et al., 2007). Therefore, I concluded that the MFA results are due to reduced G6PDH activity as a consequence of benzoate catabolism instead of increase in gluconokinase activity.

In the TCA cycle, the glyoxylate shunt was activated in the presence of benzoate. The MFA model indicated that activation of the glyoxylate shunt in cells grown on the glucose:benzoate mixture (56.8 ± 8.7%) whereas the pathway was minimally active in the glucose-grown cells (0.6 ± 0.8%) (Fig. 3). These results were consistent with previous metabolic flux studies, which indicated that the glyoxylate shunt was not active when *P. putida* KT2440 was grown on glucose alone (Sudarsan et al., 2014, Nikel et al., 2015; Sasnow et al., 2016) (Fig 6). Furthermore, Sudarsan et al. (2016) found that the glyoxylate shunt was active (99.7%, on average) when cells were grown on benzoate alone. Due to the active glyoxalate shunt, the flux from citrate to α-KG (26.4 ± 1.4%) and α-KG to succinate (15.3 ± 1.1%) diminished when cells were grown on the glucose:benzoate mixture compared to glucose alone (93.1 ± 0.2% and 83.0 ± 0.6%, respectively) (Fig. 3). These values are in agreement with reported averaged fluxes from citrate to α-KG (19.3% and 35.1% on average, respectively) and α-KG to succinate (9.6% and 0% on average, respectively) in previous metabolic flux studies in which *P. putida* KT2440 was grown on benzoate alone or a glucose succinate mixture, respectively (Sudarsan et al., 2016 and La Rosa et al., 2015, respectively). In previous studies, the accumulation of succinyl-CoA, a byproduct of benzoate catabolism, was shown to inhibit ICDH activity in liver cells (Smith et al., 1973; Tretter et al., 2005). Furthermore, TCA cycle intermediates (i.e. glyoxylate and OAA) were shown to inhibit ICDH in *P. aeruginosa* (Tiwari and Campbell, 1969). Previous studies have hypothesized that the activation of the glyoxylate shunt led to decreased ICDH activity in *P. putida* KT2440 and *E. coli* (Nikel et al., 2014 and Walsh and Koshland, 1985, respectively). Therefore, ICDH serves as a branch point for TCA cycle metabolism, in which the decreased ICDH activity occurs in concert with activation of the glyoxylate shunt (Walsh

and Koshland, 1985; Nikel et al., 2014). This will be discussed further in the following section, where kinetic flux profiling was used to elcuidate the decrease in ICDH activity in response to benzoate catabolism (see *Section* 3.4).

The net effect of the incoming carbon from succinate via the *ortho*-pathway and the glyoxylate shunt increased the flux from succinate to fumarate (131 ± 7.3%), fumarate to malate (132 ± 7.2%), and malate to OAA (104 ± 7.2%) compared to the glucose-only condition (83.5 ± 1.4%, 84.9 ± 0.8%, and 43.1 ± 1.5%, respectively) (Fig. 6). In previous metabolic flux study, Sudarsan et al. (2014) determined that these fluxes increased when *P. putida* KT2440 was grown on benzoate alone compared to when it was grown on fructose or glucose alone. Our findings were also consistent with previous proteomics findings in which succinyl-CoA synthase (succinyl-CoA to succinate) and SDH (succinate to fumarate) were upregulated when *P. putida* KT2240 was grown on benzoate compared to growth on succinate (Yun et al., 2011).

As a result of the increased fluxes in the TCA cycle downstream of succinate, pyruvate was derived primarily from different metabolites when grown on the glucose:benzoate mixture compared to growth on glucose alone. The flux from 6-PG to pyruvate and GAP (109 ± 5.4%), PEP to pyruvate (53.8 ± 0.7%), and malate to pyruvate (38.7 ± 4.1%) when cells were grown on glucose alone were different compared to when cells were grown on the glucose:benzoate mixture (38.2 ± 4.0%, 17.0 ± 1.8%, and 75.6 ± 9.2%, respectively) (Fig. 6). Thus, the MFA results indicated that, when grown on glucose alone, a major fraction of pyruvate was derived from the ED pathway via the splitting of 6-PG (54.3 ± 2.7%) with relatively smaller contributions from PEP (26.6 ± 0.3%) and malate (19.1 ± 2.0%) (Fig. 6). However, during feeding on both glucose and benzoate, pyruvate was primarily derived from malate (57.8 ± 7.0%), a TCA cycle intermediate, and smaller contributions from PEP (13% ± 1.4%) and 6-PG (29.1 ± 3.1%) (Fig. 6). In a previous FBA study, *P. putida* KT2440 appeared to deal with carbon overflow in the TCA cycle by converting OAA to pyruvate when cells were grown on benzoate alone (Sudarsan et al., 2014). However, important

metabolic fluxes towards pyruvate were not determined (Sudarsan et al., 2014). In the absence of metabolite modeling to aid in resolving the metabolic network modeling, the important flux from malate to pyruvate was omitted in this previous study. The activity of MALDH, which catalyzes the decarboxylation of malate to pyruvate and is subjected to regulation by the Crc protein, has been shown to direct carbon overflow from the TCA cycle towards gluconeogenesis in *P. putida* K2440 (La Rosa et al., 2015). Therefore, my MFA results regarding the biosynthetic fluxes for pyruvate implied increased MALDH activity in order to divert excess carbons from the TCA cycle due to benzoate catabolism (Fig. 6).

3.4. Kinetic flux profiling of the TCA cycle in response to benzoate

A switch-substrate kinetic flux experiment was conducted to investigate changes in the *in vivo* enzyme activity within the TCA cycle in response to transfer of the cells from feeding on [U-$^{13}C_6$]-glucose to feeding on nonlabeled benzoate (Fig. 7). The data from switch-substrate labeling demonstrated that glucose-grown *P. putida* KT2440 decreased the flux through ICDH, which catalyzes the catabolism of isocitrate to α-KG, in response to feeding on benzoate. The metabolites isotopically enriched with ^{13}C were expected to be populated increasingly by nonlabeled fractions due to influx of nonlabeled benzoate-derived carbons via acetyl-CoA and succinyl-CoA through the *ortho* pathway (Fig. 1). Accordingly, there was a rapid increase in nonlabeled fraction of the succinate pool wherein, after only 30 min and 60 min, the nonlabeled fraction was respectively 68.3 ± 5.4% and 78.1 ± 1.2% (Fig. 7A). The subsequent metabolites in the TCA cycle (fumarate, malate, and citrate) also became rapidly nonlabeled in a similar fashion after 30 min (76.0 ± 2.7%, 78.5 ± 18.7%, and 73.2 ± 21.9%, respectively) and after 60 min (81.9 ± 15.5%, 84.6 ± 14.3%, and 84.5 ± 16.3%, respectively) (Fig. 7A). However, by comparison, the kinetic incorporation of nonlabeled carbons into the α-KG pool was slower (Fig. 7A). Specifically, after 30 min and

60 min, the fractional pool of α-KG that was nonlabeled was only 21.1 ± 7.3% of and 32.0 ± 3.0%, respectively (Fig. 7A). The metabolite levels before and after the substrate switch were also monitored (Fig. 7B). The levels of succinate, fumarate, and citrate remained at the same level for the first 15 minutes following the substrate switch whereas the level of α-KG immediately decreased after only 15 seconds (Fig. 7B). These results thus implied that the decreased ICDH flux reported for the MFA of the mixed-substrate compared to glucose alone was a consequence of benzoate catabolism (Fig. 7).

Previous studies have indicated that ICDH activity can be regulated via metabolic feedback inhibition (i.e. succinyl-CoA, glyoxylate, and OAA) (Tiwari and Campbell, 1969;

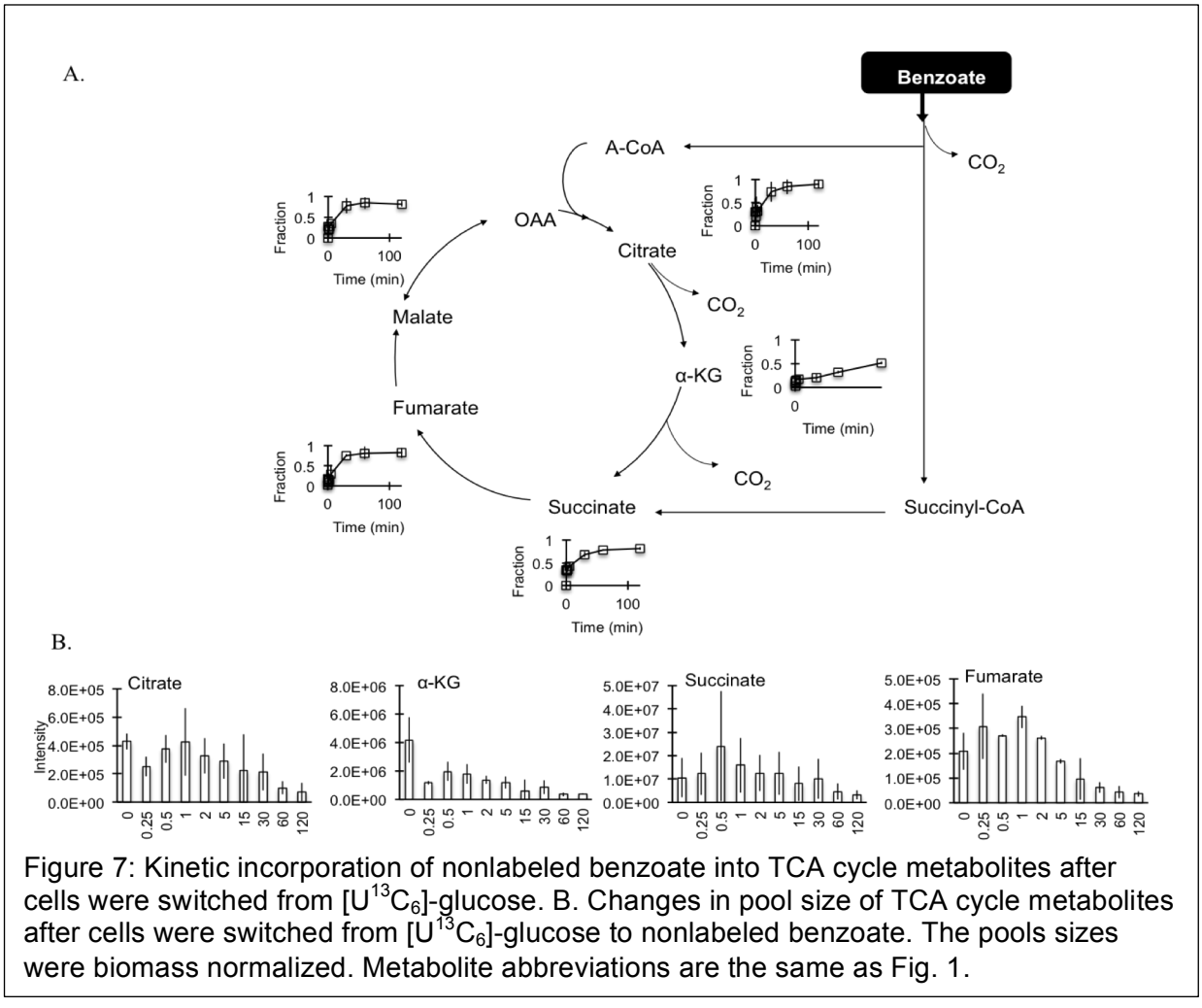

Figure 7: Kinetic incorporation of nonlabeled benzoate into TCA cycle metabolites after cells were switched from [$U^{13}C_6$]-glucose. B. Changes in pool size of TCA cycle metabolites after cells were switched from [$U^{13}C_6$]-glucose to nonlabeled benzoate. The pools sizes were biomass normalized. Metabolite abbreviations are the same as Fig. 1.

Smith et al., 1973; Tretter et al., 2005) or phosphorylation (Walsh and Koshland, 1985). It is reasonable to expect that level of succinyl-CoA would be elevated due to involvement of the *ortho* pathway in catabolizing benzoate (Fig. 1). This would explain the finding with the switch-substrate experiment (Fig. 7). And, previous studies have indicated that the activation of the glyoxylate shunt led to a decrease in ICDH activity in *P. putida* KT2440 (Nikel et al., 2014) and *E. coli* (Walsh and Koshland, 1985). The glyoxylate shunt was found to be active when *P. putida* KT2440 was grown on benzoate (Sudarsan et al. 2014; Sudarsan et al. 2016) and the *in silico* flux from citrate to α-KG was reduced in benzoate-grown cells compared to cells grown on glucose (Sudarsan et al. 2014). The MFA results also indicated an active glyoxylate shunt and a decreased flux from citrate to α-KG when cells were grown on the glucose:benzoate mixture (Fig. 7). Taken together, these results supported the hypothesis that ICDH acted as a branch point in which its decreased activity was accompanied by activation of the glyoxylate shunt (Nikel et al., 2014; Walsh and Koshland, 1985).

To investigate the implication of the decreased flux from isocitrate to α-KG for biomass precursors, the kinetic incorporation of nonlabeled carbon into Gln, an amino acid synthesized from α-KG, was also monitored (Appendix A, Fig. A9). Similar kinetic profile was obtained for the increase of nonlabeled fractions for both α-KG and Gln, indicating rapid flux from α-KG to synthesize downstream amino acids (Appendix A, Fig. A9). The metabolite pool of Gln remained stable for the first 5 min after the switch from glucose to benzoate, whereas the α-KG pool decreased within 15 s (Appendix A, Fig. A9), illustrating a delay in the effects of depleted α-KG on Gln. Further investigation is warranted to elucidate by which mechanisms benzoate catabolism induces controls on metabolic fluxes through the TCA cycle.

CHAPTER 4: CONCLUDING REMARKS

Pseudomonas putida has been previously studied for its ability to survive in diverse nutritional environments as well as its functionality in industrial applications. Within both of these contexts, *P. putida* KT2440 can utilize both sugars and aromatic substrates simultaneously as demonstrated in this study. This can give *Pseudomonas* spp. a competitive advantage in soils and can be exploited for industrial applications (Görke et al., 2008). Here both the elucidation of the metabolic network and the MFA confirmed the central hypothesis that selective substrate flux in different metabolic pathways facilitated optimal carbon metabolism. Tracking the metabolite labeling through the metabolic network revealed that glucose-derived carbon was partitioned to ED pathway and reverse EMP pathway, while benzoate-derived carbon primarily populated the TCA cycle. This suggested that carbon skeleton from benzoate was mainly oxidized in the TCA cycle, which produced reducing equivalents that are necessary in cellular respiration (Fernie et al., 2004). In addition, these results also indicated that benzoate-derived carbons were invested primarily into biomass precursors generated from TCA cycle intermediates. On the other hand, glucose-derived carbons were invested primarily in biomass precursors from the ED, reverse EMP, and PP pathways. Therefore, the carbon substrates were partitioned in different pathways to be invested into different metabolic functions. This strategy ultimately resulted in a slightly faster growth rate for cells grown on the glucose:benzoate mixture

The detailed quantitative metabolomics results obtained here revealed that several metabolic reactions in central carbon metabolism *P. putida* KT2440 were modified. Several key regulatory points were identified in the central carbon metabolism. First, G6PDH activity was decreased when cells were grown on the glucose:benzoate mixture, thereby increasing the gluconate-derived fraction in the biosynthesis of 6-PG . Second, the glyoxylate shunt was active when cells were grown on the glucose:benzoate mixture . Consequently, the fluxes from citrate to α-KG and α-KG to succinate were diminished as described previously

for succinate-grown cells, which also exhibited active glyoxylate shunt (La Rosa et al., 2015; Sudarsan et al., 2014; Sudarsan et al., 2016). Third, an increase in MALDH activity in response to carbon overflow from the TCA cycle, thus contributing to the prevalence of benzoate carbons over glucose carbon to synthesize pyruvate. The modeled fluxes quantified the changes in central carbon metabolism. However, the specific type of regulation responsible for deviations in the different carbon fluxes due to the co-metabolism of the glucose:benzoate mixture versus glucose alone could only be inferred. Connecting the elucidated changes in carbon fluxes to specific enzymatic regulation (i.e. transcriptional, translational, post-translational) warrants further investigations.

In *Saccharomyces cerevisiae*, a proteomic experiment was used to determine successfully the level of regulation for enzymes in central carbon metabolism (Oliveira et al., 2011). A similar study can be paired with the MFA results presented here to determine the level of regulation in *P. putida* KT2440 when grown in different conditions. As a significant contribution to understanding the simultaneous utilization of multiple substrates in *P. putida* KT2440, this study provides a detailed account of the intracellular metabolism for cells grown on glucose and benzoate. In soil environments, glucose and aromatics are present in natural occurring compounds or environmental contaminants (Poblete-Castro et al., 2012). In addition, lignocellulose, composed of glucose and aromatics, can be utilized as a carbon feedstock for biofuel production (Bugg et al., 2011; Fang et al., 2012; Palazzolo and Kurina-Sanz, 2016). Therefore, the new findings from this study present insights to further our understanding of soil mixed-carbon metabolism and inform the development of novel biotechnological applications in bioremediation and biofuel production.

APPENDIX A: SUPPLEMENTARY INFORMATION

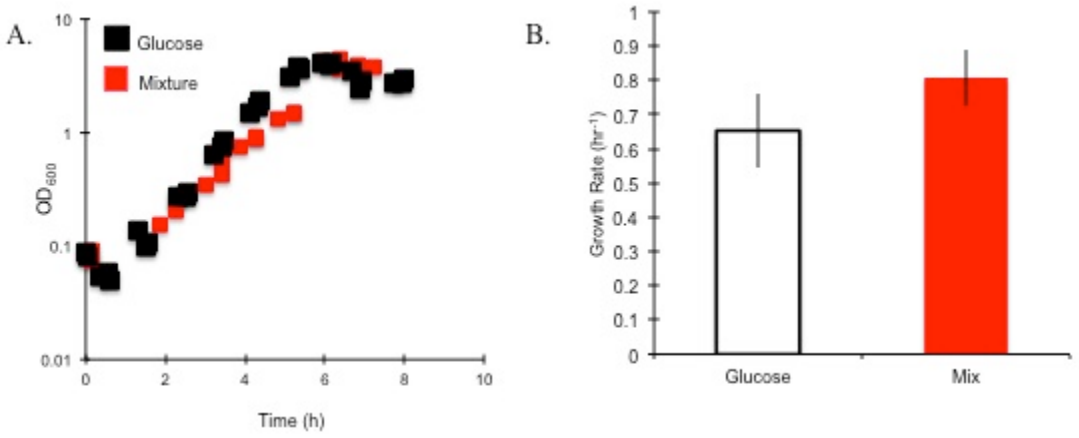

Figure A1: (A) Growth rate (h^{-1}) of *P. putida* KT2440 on glucose (100mM of C) and (B) a 50:50 mixture of glucose:benzoate (50 mM of C each) P value = 0.0099.

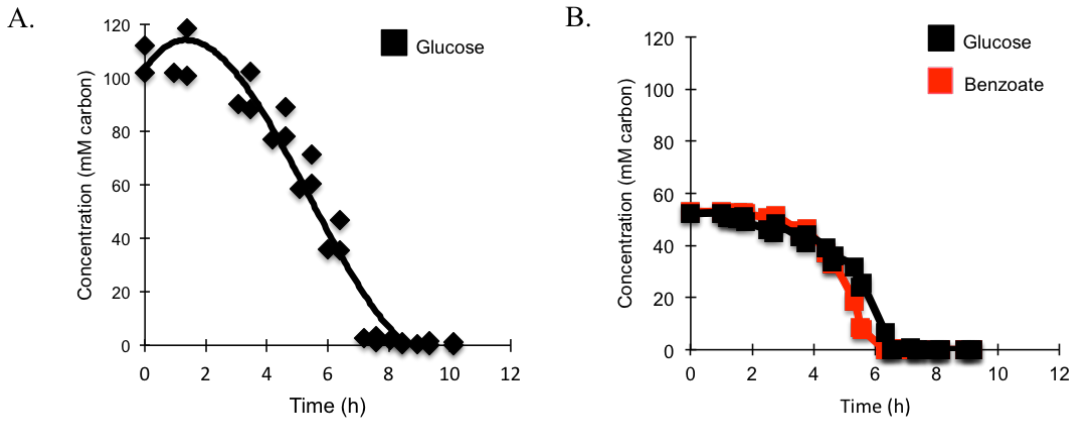

Figure A2: (A) Kinetics of extracellular substrate depletion (mM C) by *P. putida* KT2440 grown on glucose (100 mM C). (B) 50:50 mixture of glucose:benzoate (50 mM C each). To determine the consumption rate, points were used from OD 0.43 to 2.9.

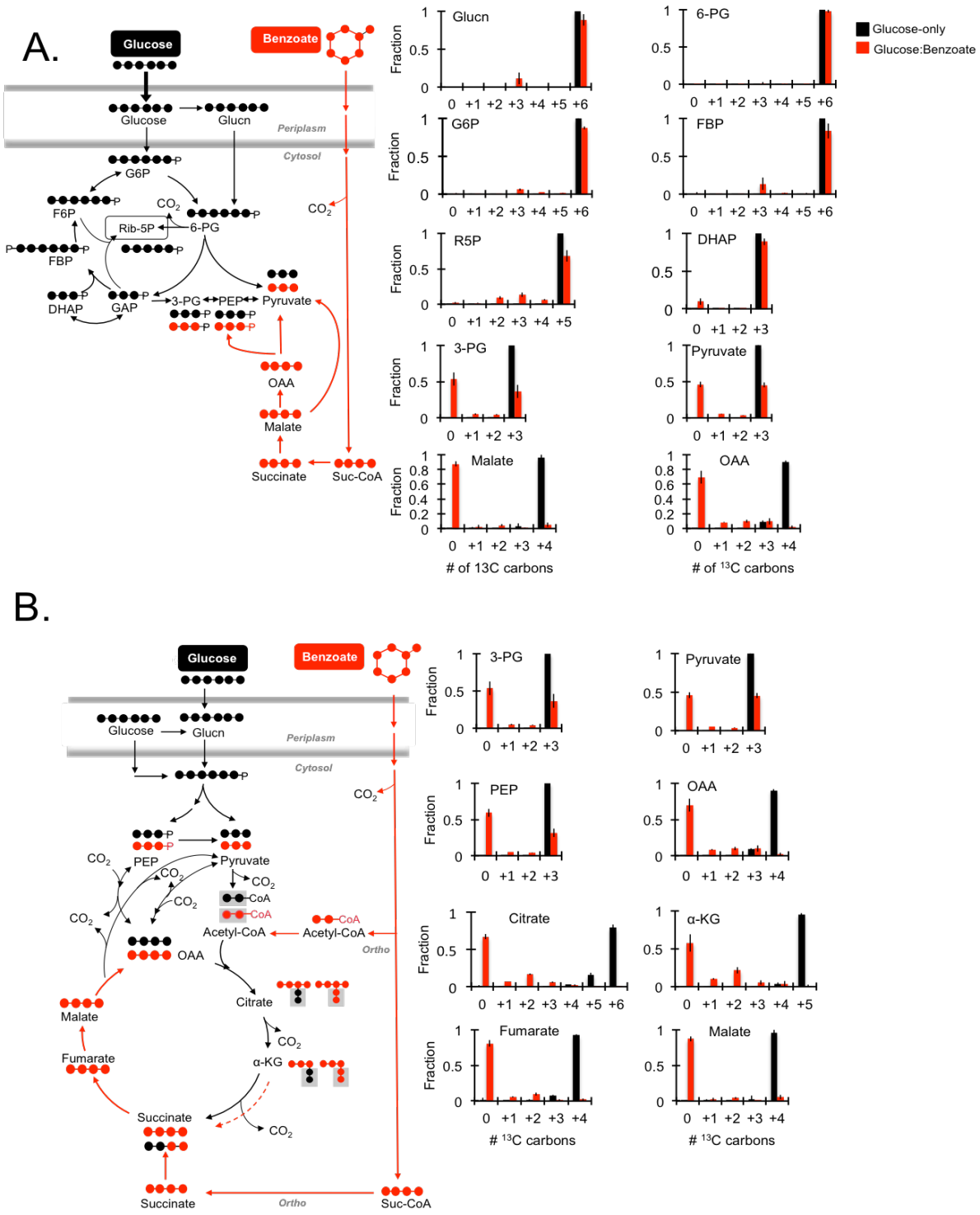

Figure A3: Comprehensive ^{13}C-labeling of metabolites in central carbon metabolism during growth on [U-$^{13}C_6$]-glucose and unlabeled benzoate in the (A) ED pathway and reverse EMP pathway and (B) TCA cycle. Metabolite abbreviations are the same as Fig. 1.

In accordance with the incorporation of [U-$^{13}C_6$]-glucose, the metabolites involved in the initial catabolism of glucose, ED pathway, and reverse EMP pathway were near fully ^{13}C-labeled with the following fraction on average: gluconate (97.8%), 6-PG (88.7%), G6P (87.5%), F6P (80.8%), FBP (83.3%), and DHAP (89.0%) (Fig. A3A). Yet, triply ^{13}C-labeled hexose-phosphates, FBP (13.3%) and G6P (6.3%), and nonlabeled DHAP (9.6%) indicated that a small fraction of C derived from benzoate was present in the reverse EMP pathway and ED pathway (Fig. A3A).

Though metabolites in the ED pathway and reverse EMP pathway were derived primarily from glucose, the ^{13}C-labeling patterns of pyruvate, PEP, and 3-PG revealed that C derived from benzoate was present downstream of the ED pathway (Fig. A3A). Pyruvate, PEP, and 3-PG were 46.1%, 31.7%, 36.5% triply ^{13}C-labeled, respectively, which was derived from glucose (Fig. A3A) Furthermore, pyruvate, PEP, and 3-PG were 45.2%, 59.3%, and 53.8% nonlabeled on average, respectively, which was derived from benzoate (Fig. A3A). Consistent with these results, del Castillo et al. (2007) reported the presence of toluene-derived carbons in serine, an amino acid derived from 3-PG, when *P. putida* KT2440 (pWW0) was grown on both toluene and glucose. Benzoate-derived carbon can be introduced to these metabolite pools when TCA cycle intermediates are converted to pyruvate or PEP through peripheral pathways (i.e. malate to pyruvate or OAA to PEP) (Fig. A3A). Subsequently, benzoate-derived carbon can enter the ED pathway, reverse EMP pathway, and PP pathway if 3-PG is converted to GAP and, subsequently, to DHAP (Fig. A3A). However, a low abundance of nonlabeled DHAP (9.6%) indicated that GAP was primarily derived from 6-PG, not 3-PG (Fig. A3A). Therefore, as previously discussed, benzoate-derived carbon was not incorporated substantially into the reverse EMP pathway or ED pathway (Fig. A3A).

The ^{13}C-labeling patterns of metabolites indicated that benzoate-derived carbons primarily populated the TCA cycle (Fig. A3B). Citrate was primarily nonlabeled (67.0%), which is in agreement with the combination of nonlabeled acetyl-CoA with nonlabeled OAA

(Fig. A3B). Citrate was also 17.8% doubly ^{13}C-labeled, which represented the fraction derived from nonlabeled OAA (69.8%) and doubly ^{13}C-labeled acetyl-CoA or doubly ^{13}C-labeled OAA (9.8%) and nonlabeled acetyl-CoA (Fig. A3B). Citrate was formed when acetyl-CoA was combined with OAA (Fig. A3B). Acetyl-CoA was derived from the ED pathway or *ortho*-pathway. From the ED pathway, nearly equal amounts of nonlabeled (46.1%) and doubly ^{13}C-labeled (45.2%) pyruvate presumably produced nonlabeled and dually labeled acetyl-CoA, respectively (Fig. A3B). In addition, nonlabeled acetyl-CoA was produced from the *ortho*-pathway, further enriching the pool of nonlabeled acetyl-CoA (Fig. A3B). As expected, the decarboxylation of citrate formed nonlabeled (57.8%), singly (10.1%), and doubly (21.6%) ^{13}C-labeled α-KG (Fig. A3B). Therefore, I concluded that the ^{13}C-labeling patterns of citrate and α-KG in the TCA cycle were consistent with the canonical routing of carbon and indicated that citrate and α-KG were composed of carbons derived from glucose and benzoate (Fig. A3B). In agreement with these findings, del Castillo et al. (2007) reported that glutamate, an amino acid derived from α-KG, consisted of carbons from both toluene and glucose when *P. putida* KT2440 (pWW0) was grown simultaneously on these substrates.

The influx of carbon to the TCA cycle from benzoate catabolism via the *ortho*-pathway considerably affected the ^{13}C-labeling patterns of metabolites fumarate, malate, and OAA (Fig. A3B). Fumarate, malate, and OAA were all primarily nonlabeled (80.8%, 87.6%, and 69.8%, respectively) (Fig. A3B). In addition, fumarate, malate, and OAA had a small fraction of singly (5.7%, 2.4%, 8.2%, respectively), doubly (9.8%, 4.4%, 9.8%, respectively), triply (1.6%, 0.4%, 9.9%, respectively), and quadruply (2.1%, 5.3%, 2.3%, respectively) ^{13}C-labeled fractions (Fig. A3B). Typically, we would expect to see a slight increase in the nonlabeled fraction of fumarate (80.8%), malate (87.6%) and OAA (69.8%) as compared to the nonlabeled fraction of α-KG (57.8%) due to the loss of ^{13}C-labeled CO_2 from singly ^{13}C-labeled α-KG (10.1%) through decarboxylation (Sasnow et al. 2016). However, the influx of nonlabeled succinate from the *ortho*-pathway resulted in a 23-30% increase in fraction of

nonlabeled fumarate (80.8%) and malate (87.6%) as compared to the nonlabeled fraction of α-KG (57.8%) (Fig. A3B). Further evidence that the influx of succinate from benzoate catabolism affected the ^{13}C-labeling of fumarate, malate, and OAA was the decrease in doubly ^{13}C-labeled fractions of fumarate (9.7%), malate (4.4%), and OAA (9.8%) as compared to α-KG (21.5%) (Fig. A3B). Finally, it is important to acknowledge the small increase of singly and triply ^{13}C-labeled fractions in OAA (8.1% and 9.9%, respectively) as compared to fumarate (5.7% and 1.6%, respectively) and malate (2.4% and 5.3%, respectively) (Fig. A3B). The increase in singly and triply ^{13}C-labeled fractions suggested the generation of OAA via pyruvate or PEP and will be further discussed in the following section (see *Section* 3.4).

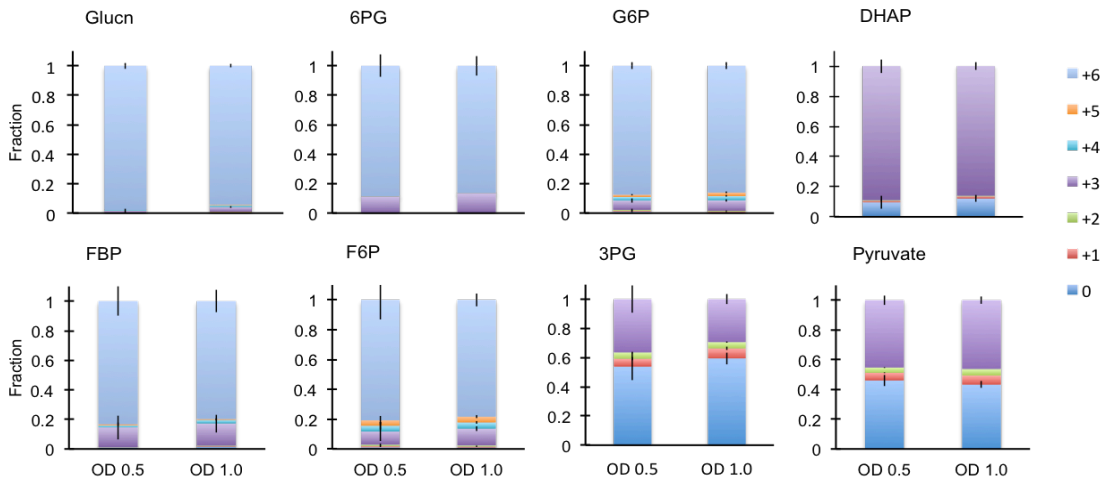

Figure A4: Labeling of the ED pathway and EMP pathway metabolites for optical density (OD) 0.5 and 1.0 during growth on [U-$^{13}C_6$]-glucose and unlabeled benzoate. Abbreviations: gluconate, Glucn; 6-phosphogluconate, 6PG; glucose-6-phosphate, G6P; dihyroxyacetone phosphate, DHAP; fructose-1,6-bisphosphate, FBP; fructose-6-phosphate, F6P; 3-phosphoglycerate, 3PG.

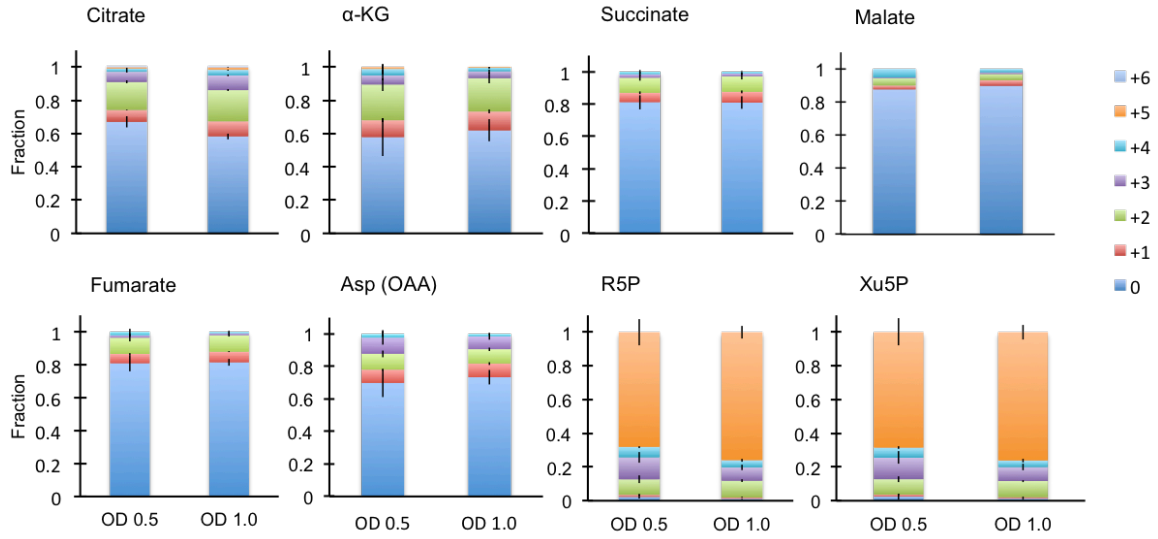

Figure A5: Labeling of the TCA cycle and PP pathway metabolites for optical density (OD) 0.5 and 1.0 during growth on [U-$^{13}C_6$]-glucose and unlabeled benzoate. Abbreviations: α-ketoglutarate, α-KG; aspartate, Asp; oxaloacetate, OAA; ribose-5-phosphate, R5P; xylulose-5-phosphate, Xu5P.

Metabolomics methods are used to detect intracellular differences in metabolic states over time as well as metabolic changes between experimental conditions (Buescher et al., 2015). Metabolomics methods are used because growth rates as well as uptake and excretion rates of microorganisms are insufficient for generating a comprehensive snapshot of metabolism (Buescher et al., 2015). For example, the rate of carbon depletion from a medium only reports how quickly cultured cells utilize a substrate. It does not elucidate how the carbon is routed intracellularly or how intracellular fluxes respond to different carbon sources (Buescher et al., 2015). These parameters of intracellular metabolism can be measured with ^{13}C-isotopic tracers both in steady-state and kinetic experiments (Sasnow et al., 2016).

An important assumption made for this experiment was that the intracellular metabolism was at a pseudo-steady state during mid-exponential phase. In pseudo-steady state experiments, biological changes are assumed to occur relatively slowly as compared to the timescale of metabolic measurement (Buescher et al., 2015). Previous experiments have shown that *P. putida* is in a pseudo-steady state when grown on single substrates (Sasnow et al., 2016). However, it has not been determined previously if cells grown in mixed-substrate conditions, especially with sugars and aromatics, remain at a pseudo-steady state during mid-exponential phase in batch cultures. To determine that a pseudo-steady state could be assumed to persist during the mid-exponential growth phase (OD 0.5 – 1.0) in this study, [U-$^{13}C_6$]-glucose and unlabeled benzoate were used to investigate the steady-state status of cellular metabolism. At OD 1.0, the concentration of metabolite pools of the TCA intermediates citrate, α-KG, succinate, and fumarate were slightly below the concentration measured at OD 0.5. In addition, the concentration of metabolites R5P of the PP pathway and FBP of the reverse EMP pathway were also slightly lower than measured at OD 1.0.

Isotopic ^{13}C-labeling for metabolites in the ED and EMP pathway indicated that glycolytic carbon was in pseudo-steady state from OD 0.5 – 1.0 (Fig. A4). In addition, isotopic ^{13}C-labeling for metabolites in the TCA cycle and PP pathways also indicated that intracellular metabolism was in a metabolic pseudo-steady state (Fig. A5). These results confirm that cells grown on glucose and benzoate in batch culture were at pseudo-steady state from OD 0.5-1.0. This condition was necessary to perform and interpret the following steady-state experiments and MFA.

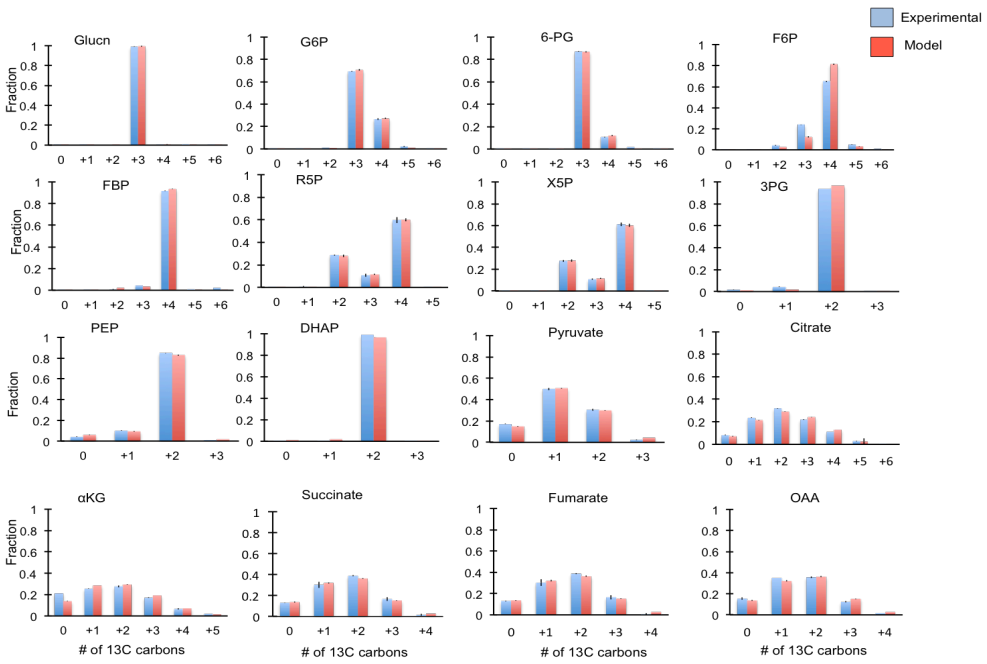

Figure A6: Model estimated (Red) and experimentally determined (Blue) of isotopomer distributions in metabolites when *P. putida* KT2440 was grown on [1,5,6 $^{13}C_3$]-glucose alone. Metabolite abbreviations are the same as in Fig. 1.

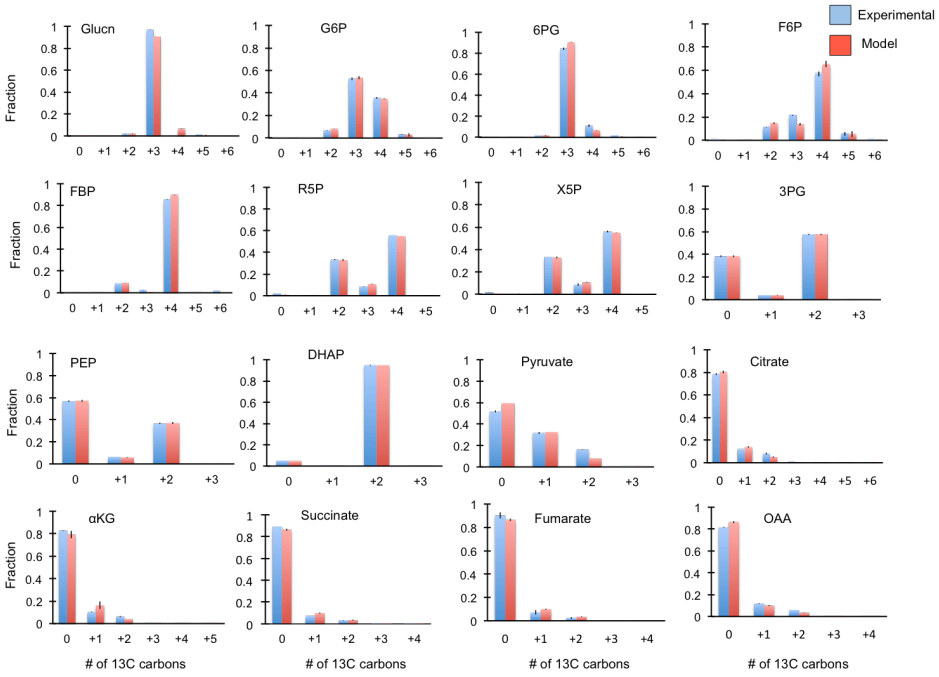

Figure A7: Model estimated (Red) and experimentally determined (Blue) of isotopomer distributions in metabolites when *P. putida* KT2440 was grown on [1,5,6 $^{13}C_3$]-glucose and benzoate. Metabolite abbreviations are the same as in Fig. 1.

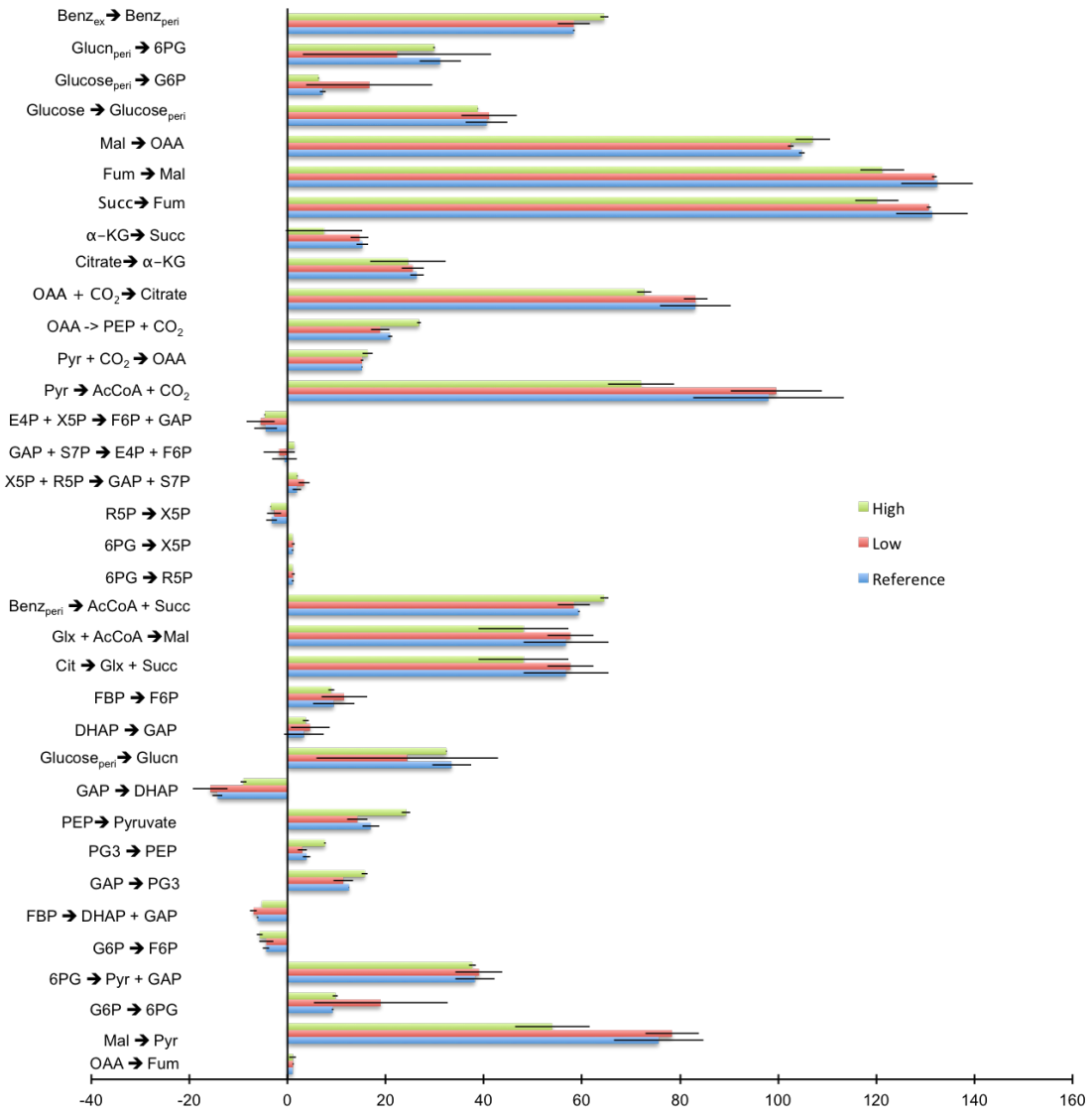

Figure A8: Changes in metabolic reaction rates in response to 100% decrease (Red) and 50% increase in contribution towards biomass compared to the rates obtained from the reference biomass comparison when *P. putida* KT2440 was grown on [1,5,6 $^{13}C_3$]-glucose and benzoate. Metabolite abbreviations are the same as in Fig. 1.

Table A1: Comparison of normalized reaction rates (%) from recent metabolic flux analysis studies. NA: indicates that no value was reported for this reaction. The black boxes indicate that the reaction is not possible. Metabolite abbreviations are the same as Fig. 1.

Condition	Gluc-only	Benz-only	Gluc:Succ	Gluc-only	Gluc:Benz
Source	Sasnow et al. 2016	Sudarsan et al. 2016	La Rosa et al. 2015	Present Study	Present study
Gluc -> $Gluc_{peri}$	100 ± 0.06		50	100 ± 1.7	40.6 ± 4.6
$Gluc_{peri}$ -> Glucn	80.6 ± 2.3	NE	NA	80.6 ± 0.0	33.4 ± 4.0
$Gluc_{peri}$ -> G6P	19.3 ± 2.3		NA	16.0 ± 6.5	7.2 ± 0.6
$Glucn_{peri}$ -> 6PG	78.0 ± 1.9		NA	79.3 ± 1.9	31.1 ± 4.2
G6P -> 6PG	34.3 ± 4.0	NA	NA	33.2 ± 3.9	9.2 ± 0.2
6PG -> Pyr + GAP	111 ± 5.7	NA	26.6	109.7 ± 5.4	38.2 ± 4.0
GAP -> PG3	64.0 ± 7.7	3.5	7.45	53.8 ± 2.2	12.5 ± 0.0
PG3 -> PEP	54.1 ± 8.0	19.6	NA	46.8 ± 1.9	3.9 ± 0.7
PEP -> Pyr	52.7 ± 6.3	25.1	NA	53.8 ± 0.7	17.0 ± 1.8
DHAP -> GAP	-22.4 ± 6.7	3.5	-7.45	-28.6 ± 2.0	-17.5 ± 1.6
FBP -> DHAP + GAP	-20.4 ± 6.6	3.5	-7.45	-25.5 ± 1.4	-6.1 ± 0.2
FBP -> F6P	20.4 ± 6.6	3.5	7.45	25.5 ± 1.4	9.4 ± 4.2
G6P -> F6P	-17.0 ± 6.5	0.29	16	-14.2 ± 1.7	-4.3 ± 0.6
6PG -> R5P	0.8 ± 0.1	NA	24.5	1.5 ± 0.4	1.1 ± 0.2
6PG -> Xu5P	0.8 ± 0.1	NA	24.5	1.2 ± 0.0	1.1 ± 0.2
R5P -> Xu5P	4.1 ± 0.1	NA	NA	-2.9 ± 0.1	-3.2 ± 1.1
Xu5P + R5P -> GAP + S7P	0.5 ± 0.0	NA	NA	1.7 ± 0.5	1.9 ± 0.9
GAP + S7P -> E4P + F6P	0.5 ± 0.0	0	NA	-3.8 ± 0.3	-0.6 ± 2.5
E4P + Xu5P -> F6P + GAP	-3.8 ± 0.1	2.6	NA	-7.4 ± 0.0	-4.5 ± 2.3
Pyr -> AcCoA + CO2	97.3 ± 0.3	130.1	2.13	108 ± 1.6	98.0 ± 15.4
OAA + AcCoA -> Cit	87.7 ± 1.7	119.0	46.8	93.7 ± 0.5	83.1 ± 7.2
Cit -> αKG	87.3 ± 1.9	19.3	35.1	93.1 ± 0.2	26.4 ± 1.4
αKG -> Succ + CO2	74.2 ± 1.8	9.6	0	83.0 ± 0.6	15.3 ± 1.1
Succ -> Fum	74.5 ± 1.6	209.1	97.9	83.5 ± 1.4	131 ± 7.3
Fum -> Mal	75. 8 ± 1.6	209.1	NA	84.9 ± 0.8	132 ± 7.2
Mal -> OAA	38.1 ± 3.0	317	2.13	43.1 ± 1.5	105 ± 7.2
Cit -> Glx + Succ	0.3 ± 0.2	99.7	NA	0.6 ± 0.8	56.8 ± 8.7
Glx + AcCoA -> Mal	0.3 ± 0.2	99.7	NA	0.6 ± 0.8	56.8 ± 8.7
OAA -> Fum	1.3 ± 0.0	NA	NA	1.4 ± 0.6	1.0 ± 0.0
Mal -> Pyr + CO2	7.5 ± 2.0	NA	14.9	38.7 ± 4.1	75.6 ± 9.2
Pyr + CO2 -> OAA	76.3 ± 2.4	179.5	NA	79.8 ± 0.6	15.2 ± 0.1
OAA -> PEP + CO2	7.5 ± 2.0	NA	NA	14.2 ± 0.3	20.9 ± 0.5
Benz -> $Benz_{peri}$		100			59.4 ± 0.2
Benz -> AcCoA + Succ		100			59.4 ± 0.2
$Succ_{ex}$-> $Succ_{intra}$			50		

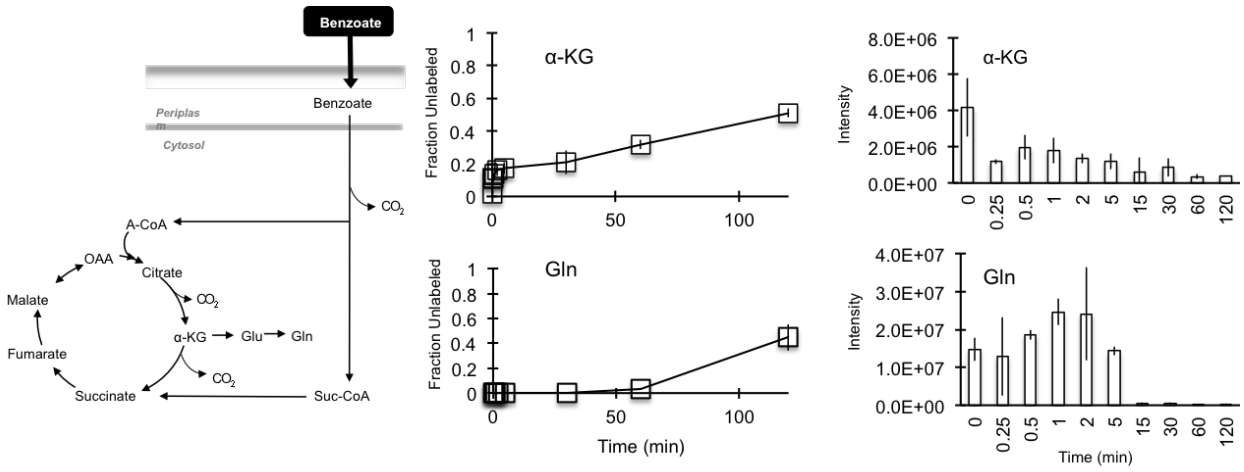

Figure A9: Kinetic incorporation of nonlabeled benzoate into α-KG and Gln after cells were switched from [$U^{13}C_6$]-glucose. Abbreviations: α-ketoglutarate, α-KG; glutamine, Gln.

APPENDIX B: FUTURE DIRECTIONS

Typical bacterial growth experiments (50 - 300 mM C) are conducted with higher carbon concentrations than those occurring in the environment (0.5 – 50 mM C) (Sasnow et al,, 2016; Sudarsan et al., 2014; Sudarsan et al., 2015; Nikel et al., 2015; Weixin et al., 1993). To test the effect of carbon concentration on growth rate, *P. putida* KT2440 was grown at several concentrations of glucose (0, 20, 50, 100, 200, 500, 1000 mM C) and the respective growth rates were determined (Fig. B1A). The growth rate increased logarithmically and plateaued for concentrations 100 – 1000 mM C. The growth rate of *P. putida* KT2440 was dependent on carbon concentration for 0 mM – 50 mM C (Fig. B1A).

Pseudomonas putida has been shown to reroute its metabolism when limited by other nutrients, such as iron (Fe) (Sasnow et al., 2016). Therefore, carbon limitation may likewise cause *P. putida* KT2440 to reroute its metabolism in order to optimize metabolism. To test this hypothesis, *P. putida* KT2440 was grown on [1,2 $^{13}C_2$]-glucose at two different concentrations: 20 mM and 100 mM C (Fig. B2). When grown on 100 mM C from glucose, *P. putida* KT2440 grew at its maximum growth rate for the medium formula used in the experiment (Fig. B1). However, when *P. putida* grew on 20 mM C from glucose, carbon was the limiting nutrient and the growth rate was 40% lower on average (Fig. B1B).

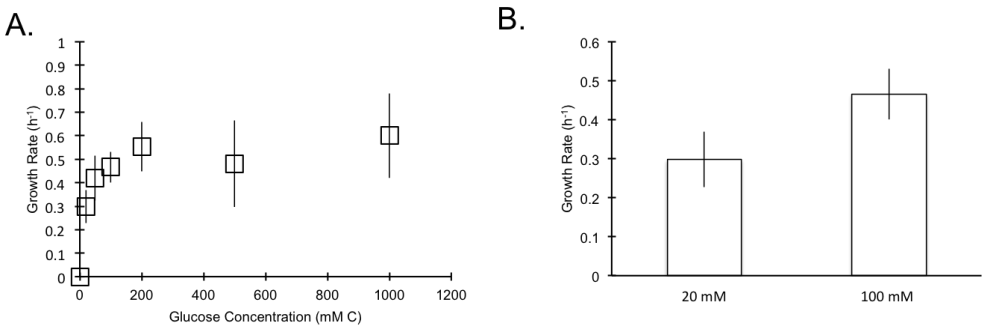

Figure B1: (A) Growth rates of *P. putida* when grown on different concentrations of glucose (0, 20, 50, 100, 200, 500, 1000 mM C). (B) Growth rates at 20 and 100 mM.

The metabolic routing of both the ED pathway and reverse EMP pathway were determined for *P. putida* KT2440 when cells were grown on [1,2 $^{13}C_2$]-glucose at 20 mM and 100 mM C (Fig. B2). Once [1,2-$^{13}C_2$]-glucose enters the periplasm, it can be oxidized to gluconate in the periplasm or phosphorylated to G6P in the cytosol. Through these reactions, both G6P and gluconate would be doubly ^{13}C-labeled (Fig. B2). Doubly ^{13}C-labeled G6P would produce doubly ^{13}C-labeled 6-PG (Fig. B2). Doubly ^{13}C-labeled gluconate would also produce doubly ^{13}C-labeled 6-PG (Fig. B2). Through the ED pathway, doubly ^{13}C-labeled 6-PG can produce doubly ^{13}C-labeled pyruvate and nonlabeled GAP (Fig. B2). Nonlabeled GAP isomerizes to nonlabeled DHAP (Fig. B2). Through the reverse EMP pathway, the nonlabeled DHAP and GAP then combine to form FBP (Fig. B2). Subsequently, nonlabeled ^{13}C-labeled FBP can produce nonlabeled F6P, which can in turn produce nonlabeled G6P (Fig. B2).

The ^{13}C-labeling patterns of metabolites in the ED pathway and reverse EMP pathway suggested that increased carbon recycling was inversely correlated with carbon concentration. For both concentrations of glucose used, gluconate was doubly ^{13}C-labeled, indicating that it was derived exclusively from glucose (Fig. B2). The ^{13}C-labeling pattern of 6-PG (nonlabeled and doubly ^{13}C-labeled) was also identical at both carbon concentrations (Fig. B2). The doubly ^{13}C-labeled 6-PG is derived from G6P and gluconate. The ^{13}C-labeling of G6P at 20 mM C revealed a differential contribution of F6P as compared to cells grown on 100 mM C (Fig. B2). The ^{13}C-labeling patterns of F6P, PEP, and pyruvate all indicated an increase in nonlabeled carbon from recycling in the ED pathway and reverse EMP pathway (Fig. B2). Pyruvate had the most striking difference with a 20.8% increase in nonlabeled carbon (Fig. B2). Therefore, when less carbon was available (20 mM C), there was more recycling of carbon through the reverse EMP pathway and ED pathway. The metabolic routing seen in 100 mM condition was therefore “luxury” metabolism, in which

carbon did have to be as conserved. The increased recycling of carbon through the reverse EMP pathway and ED pathway in the 20 mM C condition likely mirrors metabolism in natural soils, where carbon is often limited.

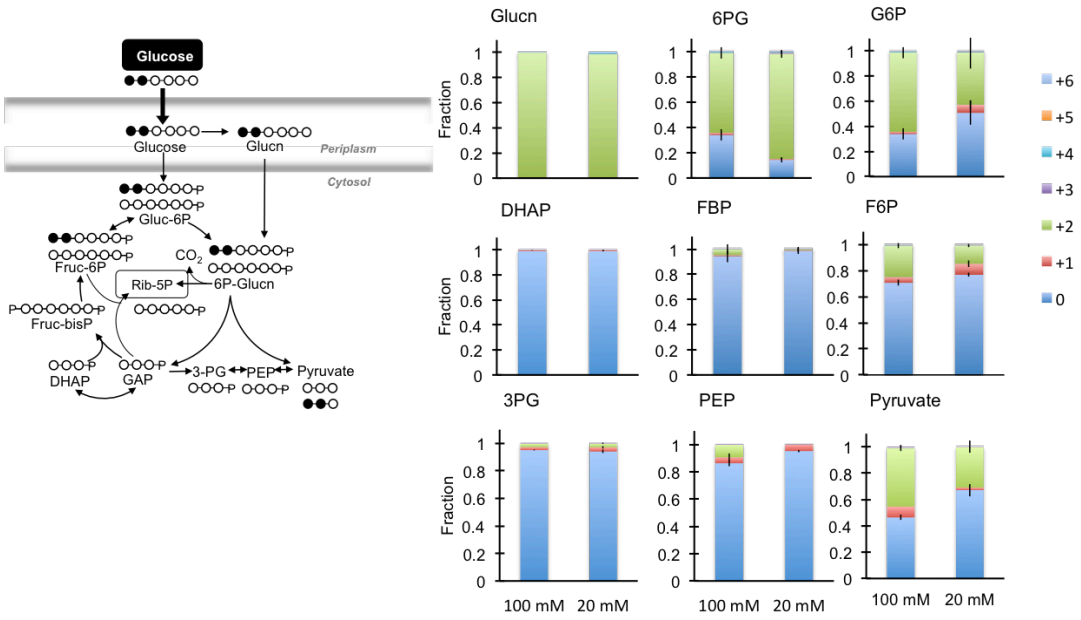

Figure B2: Steady-state labeling of the ED and EMP pathways when cells were grown on [1,2-^{13}C2]-glucose at 100 mM and 20 mM C. Abbreviations: gluconate, Glucn; 6-phosphogluconate, 6PG; glucose-6-phosphate, G6P; dihyroxyacetone phosphate, DHAP; fructose-1,6-bisphosphate, FBP; fructose-6-phosphate, F6P; 3-phosphoglycerate, 3PG.

Moisture, temperature, carbon content, and nutrient availability are constantly changing in soils, especially in agricultural systems (Walker et al., 2003; Kuzyakov et al., 2007; Blagodatskaya et al., 2008). Frequent changes in the bulk soil and rhizosphere require bacteria to constantly adjust their metabolic phenotype (Walker et al., 2003; Kuzyakov et al., 2007; Blagodatskaya et al., 2008). However, soil bacteria are also known to persist at stationary phase for long periods of time in the soil (Blagodatskaya et al., 2013). Since most metabolic experiments are conducted at steady-state, little is known about metabolism in late-exponential and stationary phases (Baudoin et al., 2002).

Therefore, studying bacterial metabolism at non-midexponential intervals (where the system is no longer at steady-state) is essential for understanding the turnover of carbon in the soil as well as calculating the resulting CO_2 outputs. Changes in metabolism over different growth phases for cells grown in batch culture were determined in order to understand how bacteria may shift their metabolism in later growth phases. Data points for OD 0.5 and 1.0 represent early- and mid-exponential phase and have been show to be at metabolic steady-state (Appendix A, Fig. A4 and A5). However, data points on the growth curve at OD 2.0 represent late-exponential phase and data points at OD 4.5 represent stationary phase, which do not represent metabolic steady-state. Both the changes in metabolite pools as well as changes in ^{13}C-labeling were measured at OD 2.0 and 4.5. Experiments were carried out using [1,2-$^{13}C_2$]-glucose for the glucose-only condition and [U-$^{13}C_6$]-glucose and nonlabeled benzoate for the glucose:benzoate condition.

As OD increased, metabolite pools levels suggested that *P. putida* partitioned carbon to biomass precursors. For the glucose-only condition, the metabolite pools were stable from OD 0.5 to 1.0 (Fig. B3). However, there was a slight increase in the metabolite pools for PEP, Citrate, and FBP (Fig. B3). From OD 0.5 to 2.0, there were more significant changes in the metabolite pools, including an increase in the PEP, α-KG, and succinate pools (Fig. B3). As extracellular glucose began to be depleted at OD 2.0, most of the metabolite pools decreased in size (Fig. B3). However, the metabolite pools that increased (PEP, α-KG, R5P, and FBP) were all pools from which biomass or ribonucleotides are derived (Fig. B3). The succinate pool also increased from OD 0.5 to 2.0. The accumulation of succinate could indicate that carbon is entering the TCA cycle to satisfy the energetic needs of the cell. Therefore, cycling slows down after the decarboxylation of citrate to α-KG and α-KG to succinate, which both generate energy. From OD 0.5 to 4.5, the same pools increased in size with the exception of FBP (Fig. B3). Therefore, either incoming glucose or

other intracellular pools may have been shunted toward PEP, α-KG, R5P, and FBP in order to increasing the cell's ability to produce biomass and ribonucleotides.

In addition, the ^{13}C-labeling patterns changed throughout the growth phases (Fig. B4). During early- and mid- exponential phase (OD 0.5 and 1.0), the ^{13}C-labeling was at isotopic steady-state as previously determined for glucose-only experiments (Sasnow et al., 2016). Since the ^{13}C-labeling at OD 0.5 and 1.0 were identical, only OD 1.0 will be referred to for the following discussion (Fig. B4). In contrast, the ^{13}C-labeling patterns changed at both OD 2.0 and 4.5 for many of the metabolites (Fig. B4). Therefore, these conditions will be referred to as separate entities. Throughout the entirety of the growth phase (OD 1.0-4.5), gluconate appeared to remain doubly ^{13}C-labeled, which is consistent with the canonical flow of glucose into the periplasm to form gluconate (Fig. B4). Both G6P and 6-PG increased in nonlabeled carbon, indicating that there was an increased routing of carbon from the reverse EMP pathway to the ED pathway (Fig. B4). This increase suggested that carbon cycling increased in the ED pathway and reverse EMP pathway when extracellular carbon was low or depleted.

Metabolites in the PP pathway suggested that there was an increased contribution from the oxidative PP pathway as OD increased. R5P and S7P increased in singly ^{13}C-labeled carbon from OD 1.0 to 4.5 (Fig. B4). Doubly ^{13}C-labeled 6-PG can be decarboxylated to form singly ^{13}C-labeled R5P and S7P. This is an indication that these metabolites are being produced from the oxidative pathways via 6-PG, instead of the nonoxidative pathway via GAP and F6P. Though the cell loses a carbon through the production of CO_2, NADPH is generated via the oxidative pathway (Sasnow et al., 2016). The TCA cycle may not have been as active as extracellular carbon was depleted, which was suggested by the decreased pools of citrate and fumarate (Fig. B3). Therefore, the cell may be energetically compensating by producing reducing equivalents through the

oxidative PP pathway. The singly ^{13}C-labeled carbon is also present in F6P, G6P, and 6-PG (Fig. B4). This indicated that F6P and GAP were produced via X5P and E4P. Taken together, these results suggested that the oxidative PP pathway was more active as extracellular carbon was depleted and OD increased.

An increase of nonlabeled carbon, generated from increased carbon cycling, was also present in the TCA cycle (Fig. B4). Citrate, α-KG, and OAA all increased in nonlabeled carbon as OD increased from 1.0 to 4.5 (Fig. B4). There was also a slight increase in nonlabeled carbon from citrate to α-KG (Fig. B4). This was consistent with the decarboxylation of singly ^{13}C-labeled citrate to form α-KG. Subsequently, the fraction of nonlabeled carbon increased from α-KG to OAA (Fig. B4), which was consistent with the decarboxylation of singly ^{13}C-labeled α-KG to form nonlabeled OAA. Therefore, these results were consistent with the canonical flow of carbon through the TCA cycle and suggested that there was no rerouting of the TCA cycle as a function of extracullular carbon depletion or an increase in OD.

For the glucose:benzoate condition, the metabolite pools were stable from OD 0.5 to 1.0, with the exception of gluconate (Fig. B5). The increase in the gluconate pool likely indicated that more glucose was coming into the cell than could be processed. This behavior has been as observed previously under Fe-starved conditions, in which gluconate was secreted (Sasnow et al., 2016). At OD 2.0, the gluconate pool remained elevated while the pool of 6-PG increased (Fig. B5). However, G6P and F6P pools decreased. When the majority of benzoate was depleted at OD 4.5, the pools of G6P and F6P recovered while 6-PG decreased (Fig. B5). Taken together, these results suggested that gluconate might be stored in the cell until benzoate is depleted. This will be discussed further in the following paragraph.

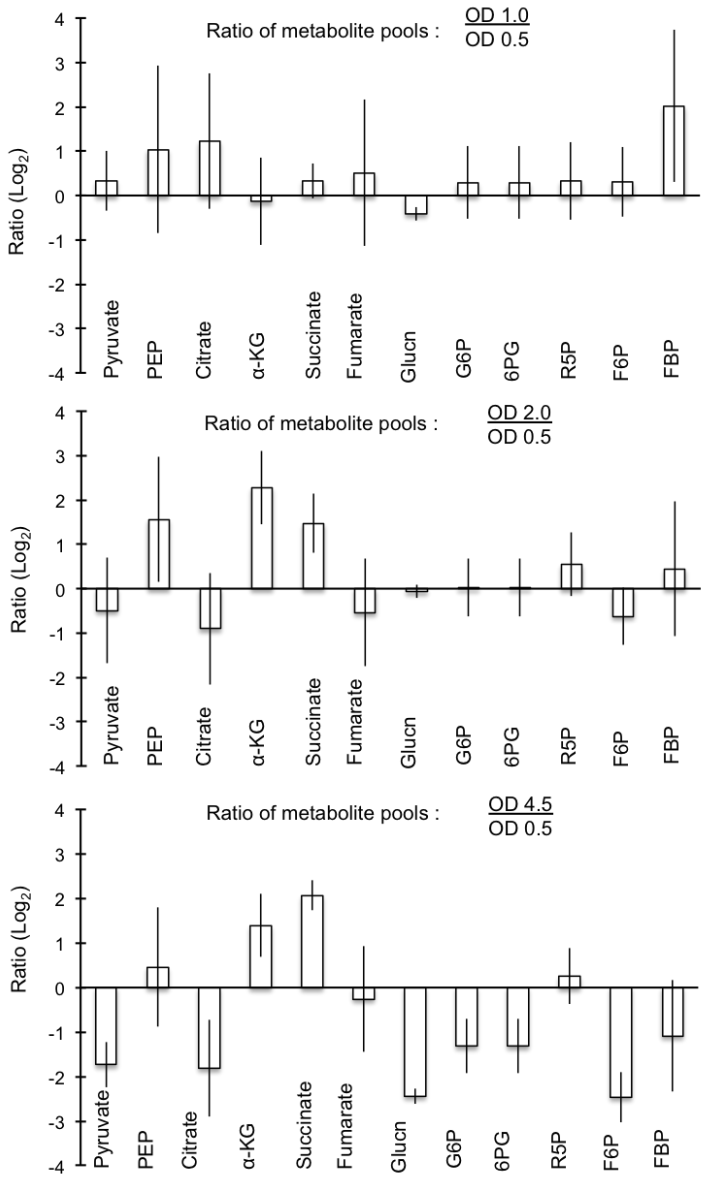

Figure B3: Metabolite pool at OD 0.5, 1.0, 2.0 and 4.5 relative to OD 0.5 for cells grown on [1,2-$^{13}C_2$]-glucose (100mM C). Abbreviations are as follows: phosphoenolpyruvate, PEP; α-ketoglutarate, α-KG; gluconate, Glucn; 6-phosphogluconate, 6PG; glucose-6-phosphate, G6P; ribose-5-phosphate, R5P; fructose-1,6-bisphosphate, FBP; fructose-6-phosphate, F6P

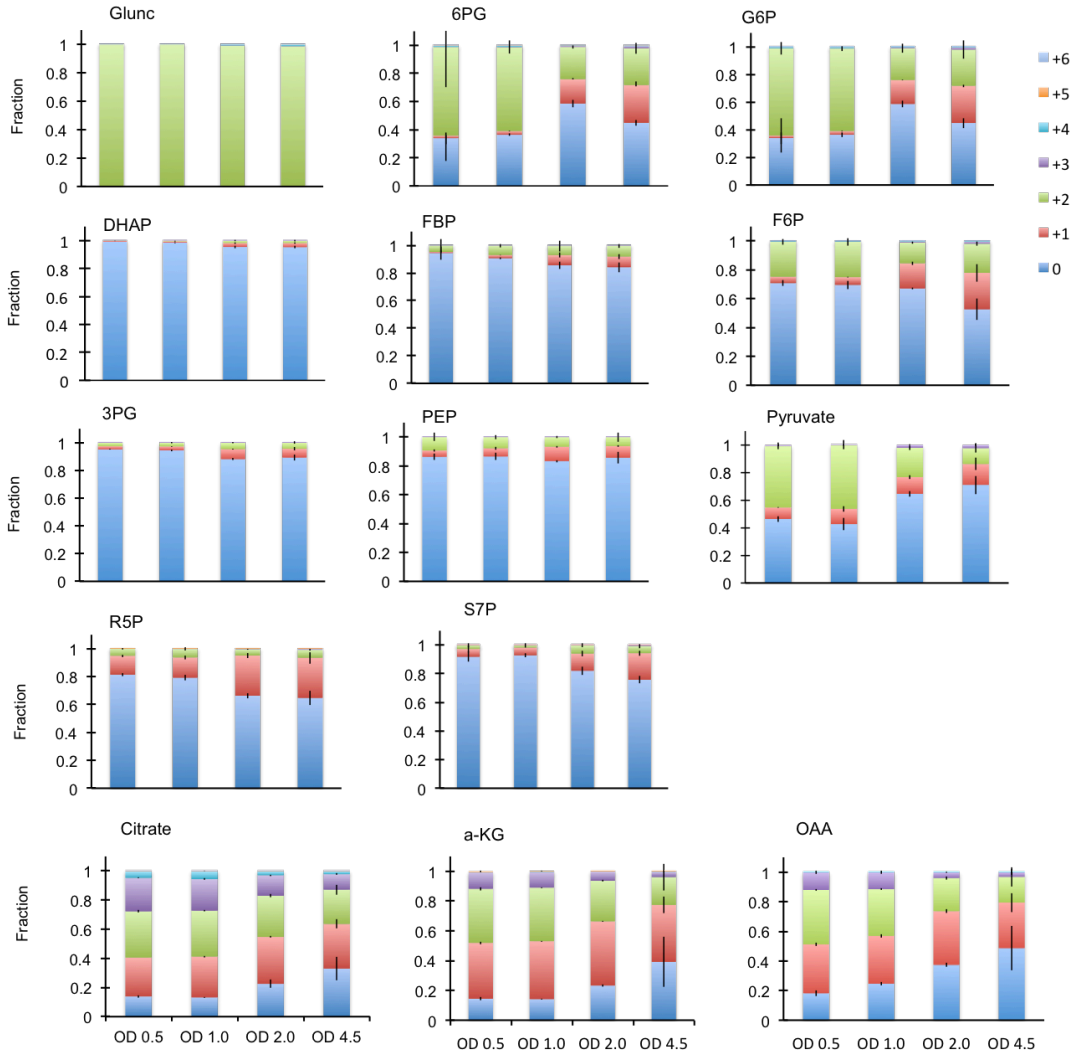

Figure B4: ^{13}C-labeling patterns of metabolites for OD 0.5, 1.0, 2.0 and 4.5 for cells grown on [1,2-$^{13}C_2$]-glucose (100 mM C). Abbreviations are as follows: gluconate, Glucn; ; 6-phosphogluconate, 6PG; glucose-6-phosphate, G6P; dihydroxyacetone phosphate, DHAP; fructose-1,6-bisphosphate, FBP; fructose-6-phosphate, F6P; 3-phosphoglycerate, 3PG; phosphoenolpyruvate, PEP; oxaloacetate, OAA.

For the glucose:benzoate condition, it was previously discussed that metabolic steady-state was from OD 0.5 – 1.0 (Appendix A, Fig. A4 and A5). However, changes in metabolism were observed for OD 2.0 and 4.5 (Fig. B6). At OD 2.0 and 4.5, more glucose entered central carbon metabolism as benzoate was depleted (Fig. B6). Throughout OD 0.5

– 4.5, gluconate remained fully unlabeled. At OD 2.0 and OD 4.5, 6-PG, G6P, FBP, F6P were all fully ^{13}C-labeled in contrast to being 10% triply ^{13}C-labeled at OD 1.0 (Fig. B6). This indicated that these metabolites no longer contained any benzoate-derived carbon. The fractions of fully ^{13}C-labeled R5P, X5P, and S7P increased from OD 1.0 to 4.5 by 34%, so that 98% of each compound was fully ^{13}C-labeled (Fig. B6). This also indicated that benzoate-derived carbon was no longer present in the PP pathway at OD 2.0 and 4.5. The ^{13}C-labeling of 3-PG, PEP, and pyruvate also changed at OD 2.0 and 4.5 (Fig. B6). For each of these metabolites, the fraction of triply ^{13}C-labeled carbon increased dramatically, 3PG (62%, on average), PEP (61%, on average), and pyruvate (31%, on average) (Fig. B6). Although the fraction of triply ^{13}C-labeled carbon in pyruvate increased by 31%, the fraction of nonlabeled, singly ^{13}C-labeled, and doubly ^{13}C-labeled pyruvate remained at 23% (Fig. B6). This indicated that pyruvate still contained benzoate-derived carbon, likely from OAA or malate. Taken together, these results indicated that glucose was the main carbon source for the ED, EMP, and PP pathways at OD 2.0 and 4.5. Additionally, it is possible that singly ^{13}C-labeled CO_2 could be responsible for an increase in ^{13}C-labeling in these pathways. In the extracellular medium at OD 2.0, 15 mM C from glucose and 7 mM C from benzoate remained. The higher concentration of glucose relative to benzoate may explain why glucose was more abundant in the ED pathway, reverse EMP pathway, and PP pathway. At OD 2.5, benzoate is depleted from the extracellular medium, while glucose persisted until OD 4.5. However, cells continued to grow on what appears to be glucose-derived carbon until OD 3.0. This suggested that cells were storing glucose-derived carbon during the growth phase. Cells could possibly be storing glucose-derived carbon as gluconate or as a polysaccharide. However, more work needs to be done to substantiate this hypothesis.

At steady-state (OD 0.5 and 1.0), benzoate-derived carbon populated the TCA cycle (Fig. B5). However, as OD increased, more glucose-derived carbon entered the TCA cycle (Fig. B5). At OD 1.0, nonlabeled carbon from benzoate comprised the majority of metabolites in the TCA cycle, especially succinate, fumarate, and OAA (Fig. B5). However, a large portion of ^{13}C-labeled carbon entered the TCA cycle at OD 2.0 and 4.5 (Fig. B5). At OD 2.0 and 4.5, citrate was composed of nonlabeled (36% and 40%, respectively), quintuply ^{13}C-labeled (22% and 17%, respectively), quadruply ^{13}C-labeled (12 and 22%, respectively), and triply ^{13}C-labeled (12 and 10%, respectively) (Fig. B5). The nonlabeled carbon was from benzoate, which entered the TCA cycle as succinyl-CoA and acetyl-CoA via the *ortho*-pathway. The quintuply ^{13}C-labeled carbon came from triply ^{13}C-labeled OAA that combined with doubly ^{13}C-labeled acetyl-CoA. Likewise, the quadruply and triply ^{13}C-labeled came from doubly and singly ^{13}C-labeled OAA combining with doubly ^{13}C-labeled acetyl-CoA. The overwhelming presence of these ^{13}C-labeled fractions of citrate and decrease in the fraction of nonlabeled citrate suggested that the pool of acetyl-CoA is mostly doubly ^{13}C-labeled at OD 2.0 and 4.5 (Fig. B5). The ^{13}C-labeled fractions of α-KG were in agreement with the decarboxylation of citrate. As compared to α-KG at OD 2.0 and 4.5, the fraction of nonlabeled carbon increased 38% and 42%, respectively (Fig. B5). This indicated that there was still a flux of nonlabeled carbon coming from benzoate via the ortho-pathway. However, the fraction of nonlabeled succinate decreased from 81% at OD 0.5 and 1.0 to 48% and 42% at OD 2.0 and 4.5, respectively (Fig. B5). Therefore, the flux of nonlabeled benzoate from the *ortho*-pathway decreased as extracellular benzoate was depleted from the medium. At OD 2.0 and 4.5, succinate was 31% and 38% fully ^{13}C-labeled, respectively (Fig. B5). This suggested that the flux from α-KG to succinate increased at OD 2.0 and 4.5 as compared to OD 1.0. Finally, the fraction of nonlabeled carbon from succinate to fumarate decreased at OD 2.0 and 4.5 (Fig. B5). This indicated

that there was a non-canonical routing of carbon into the TCA cycle. Although a large fraction of fumarate is likely produced from succinate, it can also be generated from OAA. Malate can be directly produced from OAA and then can subsequently isomerize to produce fumarate. This would explain the increase in the fully ^{13}C-labeled fraction of fumarate relative to succinate. The OAA is likely being partially synthesized from pyruvate, which would explain the larger increase in the triply ^{13}C-labeled fraction (20% and 15%) as compared to fumarate at OD 2.0 and 4.5, respectively. Triply ^{13}C-labeled OAA can be generated when it is formed from triply ^{13}C-labeled pyruvate combining with a nonlabeled CO_2. In all, more carbon from glucose was present in the TCA cycle at OD 2.0 and 4.5 than at OD 0.5 and 1.0 (Fig. B5). It also appears that a non-canonical flow of carbon may be induced as the amount of glucose-derived carbon increased in the TCA cycle (Fig. B5).

These experiments explored the effect of carbon limitation and non-steady state metabolism to provide better insight in to how carbon may be cycled in environmental conditions. Growth on a lower concentration of carbon (20 mM vs. 100 mM) indicated that more carbon was cycled through the reverse EMP pathway and ED pathway. This suggested that carbon was cycled in order to conserve the limited amount of glucose-derived carbon available to the cell. A similar behavior was observed when carbon became limited at OD 2.0 and 4.5 in the glucose-only condition. The metabolite pool data suggested that carbon may have been shunted to both biomass precursors as well as ribonucleotide synthesis. For the glucose:benzoate condition, more glucose entered metabolism in the later growth phases (OD 2.0 and 4.5). Taken together, these results suggested that metabolism changed as a function of carbon limitation. These results also revealed that performing growth and ^{13}C-labeling experiments with high carbon concentrations may not accurately represent intracellular carbon cycling in soil environments In addition, observing metabolic rerouting at metabolic steady-state may also misrepresent the intracellular

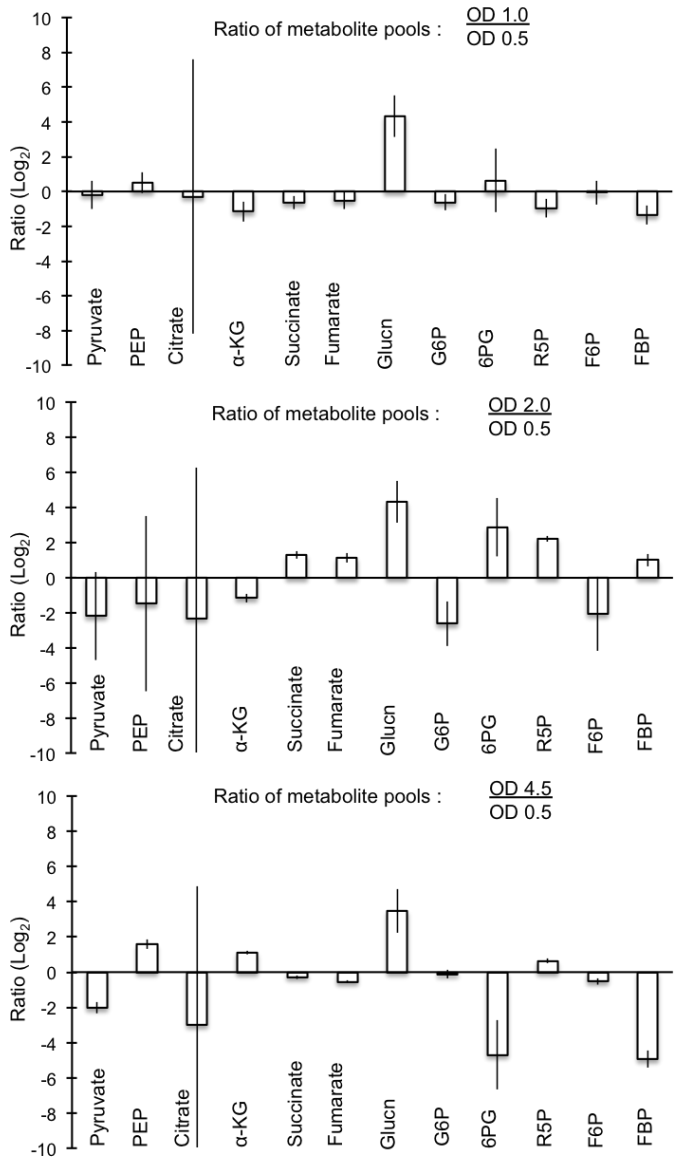

Figure B5: Metabolites pools at OD 0.5, 1.0, 2.0 and 4.5 relative to OD 0.5 for cells grown on [U-$^{13}C_6$]-glucose and unlabeled benzoate (100mM C). Abbreviations are as follows: Glucn; 6-phosphogluconate, 6PG; glucose-6-phosphate, G6P; ribose-5-phosphate, R5P; fructose-1,6-bisphosphate, FBP; fructose-6-phosphate, F6P.

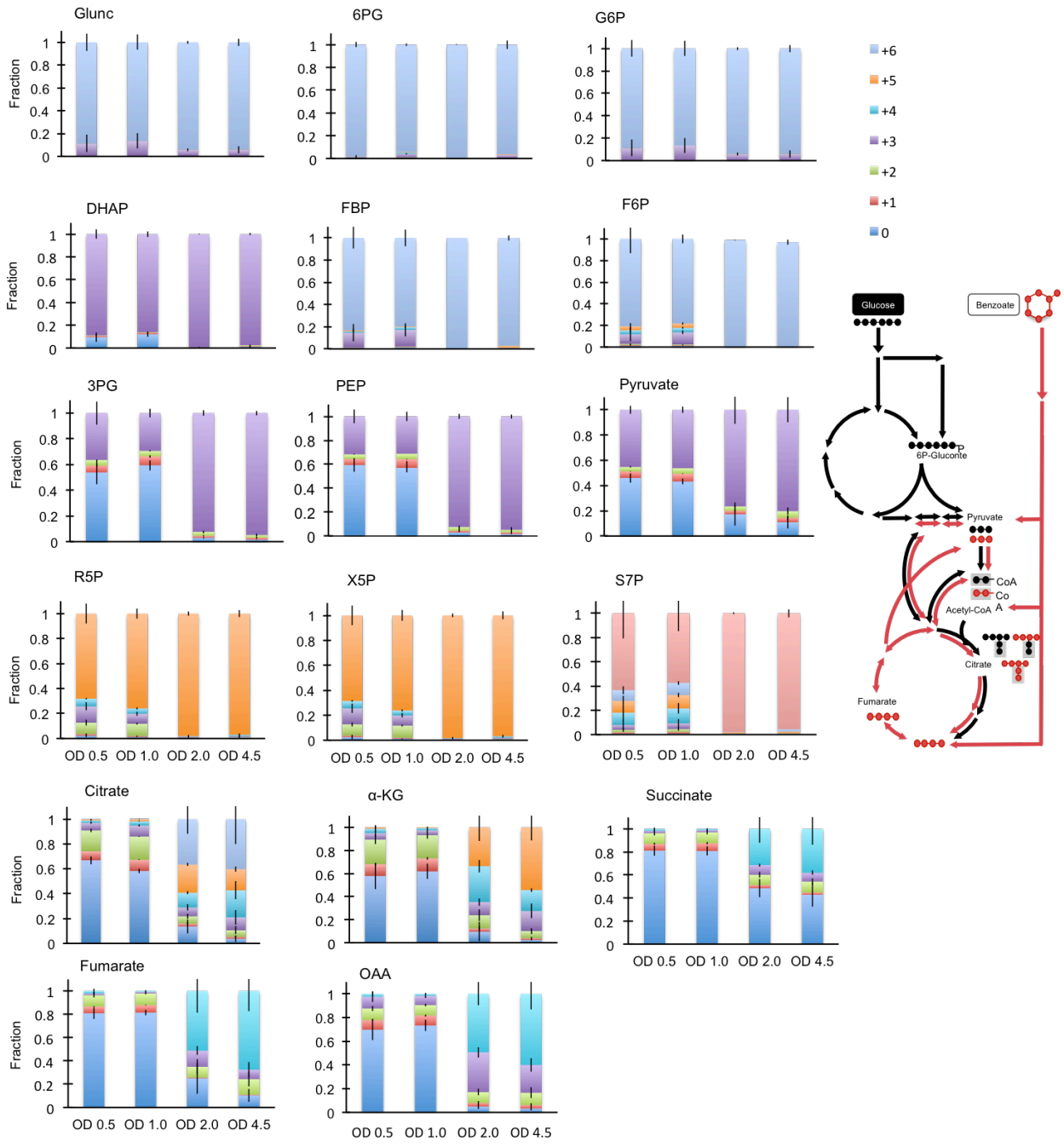

Figure B6: ^{13}C-labeling patterns of metabolites for OD 0.5, 1.0, 2.0 and 4.5 for cells grown on 50:50 mixture of [U-$^{13}C_6$]-glucose and unlabeled benzoate (50 mM C each). Abbreviations are as follows: gluconate, Glucn; 6-phosphogluconate, 6PG; glucose-6-phosphate, G6P; dihydroxyacetone phosphate, DHAP; fructose-1,6-bisphosphate, FBP; fructose-6-phosphate, F6P; 3-phosphoglycerate, 3PG; phosphoenolpyruvate, PEP; ribose-5-phosphate, R5P; xylulose-5-phosphate, Xu5P; sedoheptulose-7-phosphate, S7P; α-ketoglutarate, α-KG; oxaloacetate, OAA.

carbon cycling of bacteria in soil environments. Therefore, alternative experimental models that represent environmental actualities should be considered to more accurately describe intracellular carbon cycling in soils.

BIBLIOGRAPHY

Adair, E. C., Parton, W. J., and S.J. Del Grosso. 2008. Simple three pool model accurately describes pattern of long term litter decomposition in diverse climates. Global Change Biol. 14: 2636-2660.

Adamburg, K., Kask, S., Laht, T., and T. Paalme. 2003.The effect of temperature and pH on the growth of lactic acid bacteria: a pH-auxostat study. Int. J. Food Microbiol. 85:171-83.

Adour, L., Couriol, C., and A. Amrane. 2005. Diauxic growth of Penicillium camembertii on glucose and arginine. Enzyme Microb. Technol. 36:198-202.

Amador-Noguez, D., Feng, X.J., Fan, J., Roquet, N., Rabitz, H., and J.D. Rabinowitz. 2010. Systems-level metabolic flux profiling elucidates a complete, bifurcated tricarboxylic acid cycle in Clostridium acetobutylicum. J. Bacteriol. 192:4452–4461.

Andrews, S.C., Robinson, A. K., and F. Rodríguez-Quiñones. 2003. Bacterial iron homeostasis. FEMS Microbiol. Rev. 27: 215-237.

Antoniewicz, M. R. 2013. 13C metabolic flux analysis: optimal design of isotopic labeling experiments. Curr. Opin. Biotech. 24:1116-1121.

Aristilde, L., Lewis, I. A., Park, J. O., and J.D. Rabinowitz. 2015. Hierarchy in pentose sugar metabolism in Clostridium acetobutylicum. Appl. Environ. Microbiol. 81:1452–146.

Aristilde, L. 2016. Metabolite labelling reveals hierarchies in Clostridium acetobutylicum that selectively channel carbons from sugar mixtures towards biofuel precursors. Microbial. Biotech, doi:10.1111/1751-7915.12459.

Basu, A., Apte, S. K., and P.S. Phale. 2006. Preferential utilization of aromatic compounds over glucose by Pseudomonas putida CSV86. Appl. Environ. Microbiol. 72: 2226-2230.

Basu, A., Shrivastava, R., Basu, B., Apte, S.K., and P.S. Phale. 2007. Modulation of glucose transport causes preferential utilization of aromatic amino compounds in Pseudomonas putida CSV86. J. Bacteriol. 189: 7556–7562.

Baudoin, E., Benizri, E., and A. Gucket. 2002. Impact of growth stage on the bacterial community structure along maize roots, as determined by metabolic and genetic fingerprinting. Appl. Soil Ecol.. 19: 135-145.

Bugg, T.D., Ahmad, M., Hardiman, E. M., and R. Singh. 2011. The emerging role for bacteria in lignin degradation and bio-product formation. Curr. Opin. Biotech. 22: 394-400.

Blagodatskaya, E., and Y. Kuzyakov. 2013. Active microorganisms in soil: critical review of estimation criteria approaches. Soil Biol. Biochem. 67:192-211.

Blagodatskaya, E., and Y. Kuzyakov. 2008. Mechanisms of real and apparent priming effects and their dependence on soil microbial biomass and community structure: a critical review. Biol. and Fertil. Soils 45:115-131.

Bollag, J., Myers, C. J., and R.D. Minard. 1992. Biological and chemical interactions of pesticides with soil organic matter. Sci. Total Environ. 123:205-217.

Boukhalfa, H., and A. L. Crumbliss. 2002. Chemical aspects of siderophore mediated iron transport. Biometals. 15:325-339.

Bran, V., and K. Hantke. 2011. Recent insights into iron import by bacteria. Curr. Opin. Chem. Biol. 15: 328-334.

Buescher, J.M., Antoniewicz, M.R., Boros, L.G., Burgess, S.C., Bruengraber, H., Clish, C. B., DeBeradinis, R.J., Feron, O., Frezza, C., Ghesquiere, B., Gottlieb, E., Hiller, K., Jones, R.G., Kamphorst, J.J., Kibbey, R. G., Kimmelman, A. C., Locasale, J. W., Lunt, S. Y., Maddocks, O. DK, Malloy, C., Metallo, C. M., Meuillet, E. J., Munger, J., Nöh, Katharina, Rabinowitz, J. D., Ralser, M., Sauer, U., Stephanopoulos, G., St-Pierre, J.,

Tennant, D. A., Wittmann, C., Vander Heiden, M. G., Vazquez, A., Vousden, K., Young, J. D., Zamboni, N., and S. Fendt. 2015. A roadmap for interpreting 13C metabolite labeling patterns from cells. Curr. Opin. Biotech. 34:189-201.

Cao, B., and K. Loh. 2008. Catabolic pathways and cellular responses of Pseudomonas putida P8 during growth on benzoate with a proteomics approach. Biotech. Bioeng.. 101: 1297-1312.

Caux, P. Y., Kent, R. A., Tache, M., Grande, C., Fan, G. T., and D.D. MacDonald. 1993. Environmental fate and effects of dicamba: a canadian perspective. 1993. Rev. Environ.Contam. T. 133:1-58.

Chavarría, M., Nikel, P., Pérez-Pantoja, D., and V. de Lorenzo. 2013.The entner-doudoroff pathway empowers Pseudomonas putida KT2440 with a high stress tolerance to oxidative stress. Environ. Microbiol. 15:1772-785.

Clasquin, M. F., Melamud, E. and J.D. Rabinowitz. 2012. LC-MS data processing with MAVEN: A Metabolomic Analysis and Visualization Engine. Curr. Protoc. Bioinformatics 14–11.

Collier, D. N., Hager, P. W., and P.V. Phibbs Jr. 1996. Catabolite repression control in the Pseudomonads. Res. Microbiol. 147: 551-561.

Crown, S. B., and M. R. Antoniewicz. 2012. Parallel labeling experiments and metabolic flux analysis: past, present and future methodologies. 2012. Metab. Eng. 16:21-32.

del Castillo, T., and J. L. Ramos. 2007. Simultaneous catabolite repression between glucose and toluene metabolism in Pseudomonas putida is channeled through different signaling pathways. J.Bacteriol. 189: 6602–6610

de Lorenzo, V. 2008. Systems biology approaches to bioremediation. Curr. Opin. Biotech. 19:579-589.

Dungait, J. A. J., Hopkins, D. W., Gregory, A. S., and A. P. Whitemore. 2012. Soil organic matter turnover is governed by accessibility not recalcitrance. Global Change Biol. 18: 1781-1896.

Fang, W., Fang, Z., Zhou, P., Chang, F., Hong, Y., Zhang, X., Peng, H, and Y. Xiao. Evidence for lignin oxidation by the giant panda fecal microbiome. PLoS ONE 7:1-10.

Fuchs, G., Boll, M., and J. Heider. 2011. Microbial degradation of aromatic compounds – from one strategy to four. Nature Rev. Microbiol. 9:803-816.

Fuhrer, T., Fischer, E., and U. Sauer. 2005. Experimental identification and quantification of glucose metabolism in seven bacterial species. J. Bacteriol. 187:1581-1590.

Gaines, G. L., Smith, L., and E. L. Neidle. 1996. Novel nuclear magnetic resonance spectroscopy methods demonstrate preferential carbon source utilization by Acinetobacter calcoaceticus. J. Bacteriol. 178: 6833-6841.

George, K. W., and A. Hay. 2012. Less is more: reduced catechol production permits Pseudomonas putida F1 to grow on styrene. Microbiol. 158: 2781-2788.

Glick, B. R., Liu, C., L., Ghosh, S., E.B. Dumbroff. 1997. Early development of canola seedlings in the presence of the plant growth-promoting rhizobacterium Pseudomonas putida GR12-2. Soil Biol. Biochem. 29:1233-1239.

Görke, B., and J. Stülke. 2008. Carbon catabolite repression in bacteria: many ways to make the most out of nutrients. Nat. Rev. Microbiol. 6:613-624.

Healy Jr., J. B., Young, L. Y., and M. Reinhard. 1980. Methanogenic decomposition of ferulic acid, a model lignin derivative. Appl. Environ. Microbiol. 39:436-444.

Hester, K.L., Lehman, J., Najar, F., Song, L., Roe, B. A., and C. H. MacGregor. 2000. Crc is involved in catabolite repression control of the bkd operons of Pseudomonas putida and Pseudomonas aeruginosa. J. Baceriol. 182:1144-1149.

Johnson, C. W., Salvachúa, D., Khanna, P., Smith, H., Peterson, D. J., Beckman, G. T. 2016. Enchancing muconic acid production from glucose and lignin-derived aromatic compounds via increased protocatechuate decarboxylase activity. Metab. Eng. Comm. 3:111-119.

Howarth, W. 2015. Carbon cycling: the dynamics and formation of organic matter. In: Paul, E. A., editor. Soil microbiology, ecology, and biochemistry. 3rd ed. Burlington (MA): Elsevier. p. 339- 382.

Karishma, M., Trivedi, V. D., Choudhary, A., Mhatre, A., Kambli, P., Desai, J., and P.S. Phale. 2015. Analysis of preference for carbon source utilization among three strains of aromatic compounds degrading Pseudomonas. FEMS Microbiol. Lett. 362:1-7.

Kim, J., Pérez-Pantoja, D., Silva-Rocha, R., Oliveros, J.C., and V. de Lorenzo. 2015. High-resolution analysis of the m-xylene/toluene biodegradation subtranscriptome of Pseudomonas putida mt-2. Environ. Microbiol. 18:3327-3341.

Kögel-Knabner, I. 2002. The macromolecular organic composition of plant and microbial residues as inputs to soil organic matter. Soil Biol. Biochem. 34:139-162.

Kuzyakov, Y., Hill, P. W., and D. L. Jones. 2007. Root exudates components change litter decomposition in simulated rhizosphere depending on temperature. Plant Soil 290:293-305.

La Rosa, R., Nogales, J., and F. Rojo. 2015. The Crc/CrcZ-CrcY global regulatory system helps the integration of gluconeogenic and glycolytic metabolism in Pseudomonas putida. Environ. Microbiol. 17:3362-378.

Lee, S. K., Chou, H., Ham, T.S., Lee, T.S., and J.D. Keasling. 2008. Metabolic engineering of mircoorgansisms for biofuels production: from bugs to synthetic biology to fuels. Curr. Opin. Biotech. 19:556-563.

Lu, W., Clasquin, M.F., Melamud,E., Amador-Noguez, D., Caudy, A. A., and J.D. Rabinowitz. 2010. Metabolomic analysis via reversed-phase ion-pairing liquid chromatography coupled to a stand alone orbitrap mass spectrometer. Anal. Chem. 82:3212–3221.

Masai, E., Katayama, Y., and M. Fukuda. 2007. Genetic and Biochemical Investigations on Bacterial Catabolic Pathways for Lignin-Derived Aromatic Compounds. Biosci. Biotech. Biochem. 71:1-15.

Moorhead, D. L., Lashermes, G., Sinsabaugh, R. L., and M. N. Weintraub. 2013. Calculating co-metabolic cost of lignin decay and their impacts on carbon use efficiency. Soil Biol. Biochem. 66:17-19.

Nelson, K. E., Weinel, C., Paulsen, I. T., Dodson, R. J., Hilbert, H., Martins dos Santos, V. A. P., Fouts, D. E., Gill, S. R., Pop, M., Holmes, M., Brinkac, L., Beanan, M., DeBoy, R.T., Daughtery, S., Kolonay, J., Madupu, R., Nelson, W., White, O., Peterson, J., Khouri, H., Hance, I., Chris Lee, P., Holtzapple, E., Scanlan, D., Tran, K., Moazzez, A., Utterback, T., Rizzo, M., Lee, K., Kosack, D., Moestl, D., Wedler, H., Lauber, J., Stjepandic, D., Hoheisel, J., Straetz, M., Heim, S., Kiewitz, C., Eisen, J.,Timmis, K.N., Düsterhöft, A., Tümmler, B., and C. M. Fraser. 2002. Complete genome sequence and comparative analysis of the metabolically versatile Pseudomonas putida KT2440. Environ. Microbiol. 4:799-808.

Nishimura, T., Vertès, A. A., Shinoda, Y., Inui, M., and H. Yukawa. 2007. Anaerobic growth of Corynebacterium glutamicum using nitrate as a terminal electron acceptor. Appl. Microbial and Cell Physiology. 75: 889-897.

Nikel, P. I,, Kim, J., and V. de Lorenzo. 2014. Metabolic and regulatory rearrangements underlying glycerol metabolism in Pseudomonas putida KT2440. Environ. Microbiol. 16:239-54.

Nikel, P.I, Chavarría, M., Fuhrer, T., Sauer, U., and V. de Lorenzo. 2015. Pseudomonas putida KT2440 strain metabolizes glucose through a cycle formed by enzymes of the entner-doudoroff, embden-meyerhof-parnas, and pentose phosphate pathways. J. Biol. Chem. 290:25920-25932.

Nikel, P. I., Chavarría, M., Danchin, A., and V. de Lorenzo. 2016. From dirt to industrial applications: Pseudomonas putida as a Synthetic Biology chassis for hosting harsh biochemical reactions. Curr. Opin. Chem. Biol. 34:20-29.

Malhat, F., Fayz, A. E., Loutfy, N., and M.T. Ahmed. 2013. Residues and dissipation of the pesticide emamectin benzoate under Egyptian field condition: a case study. Toxicol. Environ. Chem. 95:1099-1107.

MacGregor, C.H., Wolff, J.A., Arora, S.K., Hylemon, P.B., and P.V. Phibbs. 1992. Catabolite repression control in Pseudomonas aeruginosa. In: Galli, E., Silver, S., and B. Witholt, editors. Pseudomonas: molecular biology and biotechnology. Washington (DC): Am. Soc. Micriobiol. p. 198-206.

Michalska, K., Chang, C., Mack, J. C., Zerbs, S., Joachimiak, A., and F. Collart. 2012. Characterization of transport proteins for aromatic compounds derived from lignin: benzoate derivative binding proteins. J. Mol. Biol. 423: 555-575.

Neely, J. R., Rovetto, M. J., and J. F. Oram. 1972. Myocardial utilization of carbohydrate and lipids. Prog. Cardiovasc. Dis. 15:289-329.

Oliveira, A. P., and U. Sauer. 2012. The importance of post-translational modifications regulating Saccharomyces cerevisiae metabolism. FEMS Yeast Res. 12:104-117.

Palleronia, N. 1984. Introduction to the family Pseudomonaceae. In: Starr, M. P., Stolp, H., Trüper, H. G., Balows, A., and H. G. Schlegel, editors. The prokaryotes. Baltimore (MD): Williams & Wilkins. p. 655-665.

Tengerdy, R.P., and G. Szakacs. 2003. Bioconversion of lignocellulose in solid substrate fermentation. Biochem. Eng. J. 13:169-179.

Palazzolo, M. A., and M. Kurina-Sanz. 2016. Microbial utilization of lignin: available biotechnologies for its degradation and valorization. World J. Micriobiol. Biotechnol. 32:173.

Park, J. O., Rubin, S. A., Xu, Y., Amador-Noguez, D., Fan, J., Shlomi, T., and J. D. Rabinowitz. 2016. Metabolite concentrations, fluxes and free energies imply efficient enzyme usage. Nat. Chem. Biol. 12:482-489.

Parween, M., Ramanathan, A.L., Khillare, P. S., and N. J. Raju. 2014. Persistence, variance and toxic levels of organochlorine pesticides in fluvial sediments and the role of black carbon in their retention. Environ.Sci. Pollut. R. 21:6525-6546.

Pietkäinen, J., Pettersson, M., and E. Bååth. 2005. Comparison of temperature effects on soil bacterial and fungal growth rates. FEMS Microbiol. Ecol. 75:1589-96.

Pieper, D.H., and W. Reineke. 2000. Engineering bacteria for bioremediation. Curr. Opin. Biotech. 11:262-270.

Pinton, R., Varanini, Z., and P. Nannipieri. 2007.The rhizosphere: biochemistry and organic substances at the soil-plant interface. 2nd ed. Boca Raton (FL): CRC Press.

Pirt, S.J. 1965. The maintenance energy of bacteria in growing cultures. P. Roy. Soc. Lond. 163:224-31.

Poblete-Castro, I., Becker, J., Dohnt, K., Martains dos Santos, V., and C. Wittmann. 2012. Industrial biotechnology of Pseudomonas putida and related species. Appl. Microbiol. Biotechnol. 93:2279-2290.

Rasse, D. P., Dignac, M. F., Bahri, H., Rumpel, C., Mariotti, A., and C. Chenu. 2006. Lignin turnover in an agricultural field: from residues to soil-protected fractions. Eur. J. Soil Sci. 57:530-538.

Rojo, F., Pieper, D. H., Engesser, K. H., Knackmuss, H. J., and K. N. Timmis. 1987. Assemblage of ortho cleavage route for simultaneous degradation of chloro-and methylaromatics. Sci. 238:1395-1398.

Sansnow, S.S., Wei, H., and L. Aristilde. 2016. Bypass in intracelliar glucose metabolism in iron-limited Pseudomonas putida. MicrobiologyOpen. 1:3-20.

Sapozhnikova, Y., and S.J. Lehotay. Multi-class, multi-residue analysis of pesticides, polychlorinated biphenyls, polycyclic aromatic hydrocarbons, polybrominated diphenyl ethers, and novel flame retardants in fish using fast, low-pressure gas chromatography-tandem mass spectrometry. Anal. Chim. Acta. 758:80-92.

Sasaki, T.; Ishikawa, H. Production of essential amino acids from glutamate by mycetocyte symbionts of the pea aphid, Acyrthosiphon pisum. 1995. Journal of insect physiology. 41: 41-46.

Schmidt, M. W. I., Tom, M. S., Abiven, S., Dittmar, T., Guggenberger, G., Janssens, I. A., Klber, M., Kogel-Knabner, I., Lehmann, J., Manning, D. A. C., Nannipieri, P., Rasse, D. P., Weiner, S., and S. E. Trumbore. 2011. Persistence of soil organic matter as an exosystem property. Nat. Prespect. 478:49-56.

Schimdt, A., Dordick, J.S., Hauer, B., Kiner, A., Wubbolts, M., and B. Witholt. 2001. Industrial biocatalysis today and tomorrow. Nat. 409:258-268.

Schmidt, M., and V. de Lorenzo. 2016. Synthetic bugs on the loose: containment options for deeply engineered (micro)organisms. Curr. Opin. Biotech. 38:90-96.

Silva-Rocha, R., and V. de Lorenzo. 2014. The pWW0 plasmid imposes a stochastic expression regime to the chromosomal ortho pathway for benzoate metabolism in Pseudomonas putida. FEMS Microbiol. Letters. 356:176-183.

Silva-Rocha, R., Perez-Pantoja, D., V. de Lorenzo. 2013. Decoding the genetic networks of environmental bacteria: regulatory moonlighting of the TOL system of Pseudomonas putida mt-2. ISME J. 7:229-232.

Smith, C. M., Bryla, S., and J.R. Williamson. 1974. Regulation of Mitochondial a-ketoglutarate metabolism by product inhibition of a-ketoglutarate dehydrogenase. J. Biol. Chem. 249:1497-1505.

St. John, M. G., Orwin, K. H., and I. A. Dickle. 2011. No 'home' versus 'away' effects of decomposition found in a grassland-forest reciprocal litter transplant study. Soil Biol. Biochem. 43:1482-1489.

Sudarsan, S., Blank, L.M., Dietrich, A., Vielhauer, O., Takors, R., Schmid, A., and M. Reuss. 2016. Dynamics of benzoate metabolism in Pseudomonas putida KT2440. Met. Eng. Comm. 3:97-110.

Sudarsan, S., Dethlefsen, S., Blank, L. M., Siemann-Herberg, M., and A. Schmid. 2014. The functional structure of central carbon metabolism in Pseudomonas putida KT2440. Appl. Environ. Microbiol. 80:5292-5303.

Tretter, L., and V. Adam-Vizi. 2005. Alpha-ketoglutarate dehydrogenase: a target and generator of oxidative stress. Philos. Trans. R. Soc. 360:2335 – 2345.

van Durren, J. B., Puchalka, J., Mars, A., E., Bücker, R., Eggink, G., Wittmann, C., and V. A. Martins dos Santos. 2013. Reconciling in vivo and in silico key biological parameters of Pseudomonas putida KT2440 during growth on glucose under carbon-limited condition. BMC Biotechnol. 13: doi:10.1186/1472- 6750-13-93.

Vardon, D.R., Franden, M., Johnson, C.W., Karp, E.M., Guarnieri, M.T., Linger, J.G.,

Salm, M.J., Strathmann, T.J., and G. T. Backham. 2015. Adipic acid production from lignin. Energy Environ. Sci. 8:617-628.

Walsh, K., and E. Koshland, Jr. 1985. Branch point control by the phosphorylation state of isocitrate dehydrogenase. J. Biol. Chem. 260:8430-8437.

Walker, T. S., Bais, H. P., Grotewold, E., and J. M. Vivanco. 2003. Root exudation and rhizosphere biology. Plant Physiol. 132:44-51.

Wang, C. H., Stern, I. J., and C. M. Gilmour. 1959. The catabolism of glucose and gluconate in Pseudomonas species. Biochem. Biophys. 81:489-492.

Weixin, C., Coleman, D. C., Carroll, C. R., and C. A. Hoffman. 1993. In situ measurement of root respiration and soluble C concentrations in the rhizosphere. Soil Biol. Biochem. 9:1189-1196.

Wiechert, W. 2001.13C metabolic flux analysis. Met. Eng. 3:195-206.

Wiechert, W. 2002. An introduction to 13C metabolic flux analysis. Genet. Eng. 24:215-238.

Weitzel, M., K. Noh, T. Dalman, S. Niedenfuhr, B. Stute, and W. Wiechert. 2012. 13CFLUX2 high performance software suit for 13C-metabolic flux analysis. Bioinformatics 29:143–145.

Wood, W. A. 1954. Carbohydrate oxidation by Pseudomonas fluorescens. Bacteriol. Rev. 206:625-635.

Worsey, M.J., and P. A. Williams. 1975. Metabolism of toluene and xylenes by Pseudmonas (putida(arvilla) mt-2: evidence for a new function of the TOL plasmid. J.Bacteriol. 124:7-13.

Yamaguchi, M., and H. Fujisawa. 1978. Characterization of NADH-cytochrome c reductase, a component of benzoate 1,2-dioxygenase system from Pseudomonas arvilla c-1. J. Biol. Chem. 253:8848-8853.

Yamaguchi, M., and H. Fujisawa. 1980. Purification and characterization of an oxygenase component in benzoate 1,2-dioxygenase system from Pseudomonas arvilla c-1. J. Biol. Chem. 255:5058-5063.

Yamaguchi, M., and H. Fujisawa. 1982. Subunit structure of oxygenase component in benzoate-1,2-dioxygenase system from Pseudomonas arvilla c-1. J. Biol. Chem. 257:12497- 12502.

Yun, S., Park, G. W., Kim, J. W., Kwon, S. O., Chio, C., Leem, S., Kown, K., Yoo, J. S., Lee, C., Kim, S., and S. Kim. 2011. Proteomic characterization of Pseudomonas putida KT2440 in response to a monocyclic aromatic compound by iTRAQ analysis and 1DE-MudPIT. J. Proteomics 74:620-628.

Zamboni, N, Fendt, S. M., Ruhl, M., and U. Sauer. 2009. (13)C-based metabolic flux analysis. Nat. Protoc. 4:878-892.

Zhang, D., Hui, D., Luo, Y., and G. Zhou. 2008. Rates of litter decomposition in terrestrial ecosystems: global patterns and controlling factors. J. Plant Ecol. 1:85-93.